

Learning Functional Graphs with Nonlinear Sufficient Dimension Reduction

Kyongwon Kim

Department of Applied Statistics

Department of Statistics and Data Science

Yonsei University

50 Yonsei-ro, Seodaemun-gu, Seoul, 03722, South Korea

KIMK@YONSEI.AC.KR

Bing Li

Department of Statistics

Pennsylvania State University

326 Thomas Building, University Park, PA 16802, USA

BXL9@PSU.EDU

Editor:

Abstract

Functional graphical models have undergone extensive development during the recent years, leading to a variety models such as the functional Gaussian graphical model, the functional copula Gaussian graphical model, the functional Bayesian graphical model, the nonparametric functional additive graphical model, and the conditional functional graphical model. These models rely either on some parametric form of distributions on random functions, or on additive conditional independence, a criterion that is different from probabilistic conditional independence. In this paper we introduce a nonparametric functional graphical model based on functional sufficient dimension reduction. Our method not only relaxes the Gaussian or copula Gaussian assumptions, but also enhances estimation accuracy by avoiding the “curse of dimensionality”. Moreover, it retains the probabilistic conditional independence as the criterion to determine the absence of edges. By doing simulation study and analysis of the f-MRI dataset, we demonstrate the advantages of our method.

Keywords: Functional Generalized Sliced Inverse Regression, Reproducing Kernel Hilbert Space, Nested Hilbert Space, Functional Conjoined Conditional Covariance Operator

1 Introduction

Functional data, where each observation unit is a function rather than a number or a vector, has become one of the most prevalent data forms in recent applications, as evidenced by the large amount of data produced in medical research, epidemiology, genetics, forensic science, finance, and econometrics. As a result, there have been an explosive development for functional data analysis (FDA) in the last two decades or so. See, for example, Ramsay and Silverman (2005, 2007), Yao, Müller, and Wang (2005), Ferraty and Vieu (2006), Horváth and Kokoszka (2012), and Hsing and Eubank (2015). For a comprehensive overview of the recent research, see Wang et al. (2016). A most recent advance in FDA is the functional graphical model, which is introduced to estimate networks where the observations on the vertices are random functions. This type of multivariate functional data are common in neuroimaging applications such as EEG and f-MRI. The past eight years or so have seen

momentous development of this area into several directions, such as Gaussian and copula Gaussian functional graphical models (Qiao et al., 2019, 2020; Solea and Li, 2022), Bayesian functional graphical models (Zhu, Strawn, and Dunson, 2016), nonparametric functional graphical models (Li and Solea, 2018; Solea and Dette, 2022; Lee et al., 2023b), conditional and structural functional graphical models (Lee and Li, 2022; Lee et al., 2023a), functional directed acyclic graphical models (Li et al., 2024), differential functional graphical models (Zhao et al., 2019), and functional graphical models via neighborhood selection (Zhao et al., 2024).

The functional graphical model is rooted in the classical statistical graphical model, where the observations on the vertices are numbers (Yuan and Lin, 2007; Meinshausen et al., 2006). Let $V = \{1, \dots, p\}$ be a set of nodes and E be a subset of the set of distinct pairs $V = \{(i, j) \in V \times V : i \neq j\}$. Let $G = (V, E)$ be the undirected graph with its vertices represented by the members of V and its edges by the members of E . Let $X = (X^1, \dots, X^p)$ be a random vector. A statistical graphical model is defined by the equivalence

$$(i, j) \notin E \Leftrightarrow X^i \perp\!\!\!\perp X^j | X^{-(i,j)}, \quad (1)$$

where $\perp\!\!\!\perp$ means the conditional independence and $X^{-(i,j)}$ denotes X with its i -th and j -th components removed. This equivalence means, intuitively, there is an edge between (i, j) if and only if X^i and X^j are directly related; that is, they are dependent even after removing the effects of all the other nodes. The earliest graphical models are based on the Gaussian assumption (Yuan and Lin, 2007). These were then extended to the non-Gaussian cases in a variety of ways: through copula transformation (Liu et al., 2009, 2012; Xue and Zou, 2012), through fully nonparametric estimation (Fellinghauer et al., 2013; Voorman et al., 2014), and through additive conditional independence (Li et al., 2014; Lee et al., 2016a,b).

As mentioned earlier, a data form that motivated the above mentioned extension to the functional graphical model is f-MRI data in medical research. An example is the f-MRI data collected by the ADHD consortium (Milham et al., 2012), where each vertex corresponds to a subregion of a brain consisting of a set of voxels. At each voxel, a brain signal known as the brain oxygen level dependent, or BOLD, is recorded over a time interval, which is then aggregated over the subregion to form a function over the interval. The functions for all subregions then form a vector of interdependent random functions. The functional graphical model was introduced to characterize the interdependence in the form a brain network. Figure 1 illustrates the situation: on the left is the image of a brain network plotted by the BrainNet viewer (Xia et al., 2013, <http://www.nitrc.org/projects/bnv/>), and on the right is the resting state data of one voxel from two groups of children, one with ADHD, the other without ADHD. More specifically, in the functional graphical model, we assume (X^1, \dots, X^p) to be the random functions observed at the set of voxels $\{1, \dots, p\}$. The functional graphical model is based on the same equivalence as (1) except that, here, the conditional independence is among random functions rather than scalar random variables. These relations are then estimated from a sample of observations on (X^1, \dots, X^p) , as obtained from a group of subjects.

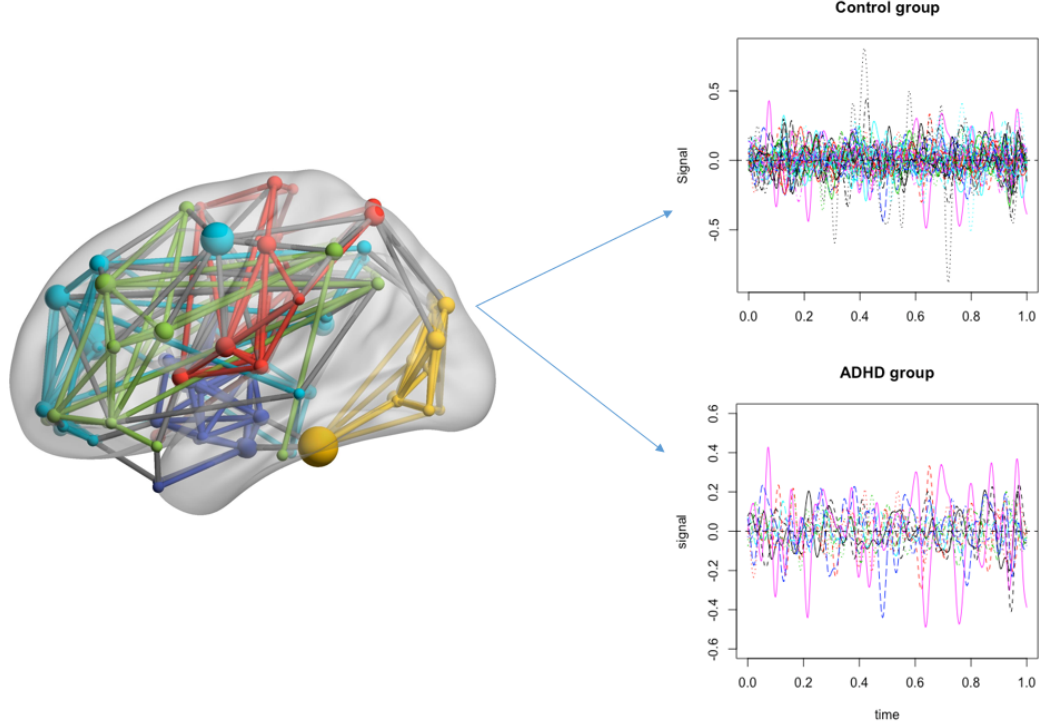


Figure 1: Example of human brain network (left) and f-MRI functional data for control group (upper right) and ADHD group (lower right).

The functional graphical model proposed by Qiao et al. (2019) is based on the assumption that (X^1, \dots, X^p) is a Gaussian random element in a Hilbert space. Their method is based on truncating the Karhunen-Loeve expansion (K-L expansion) of each X^i , and applying the group graphical Lasso (Yuan and Lin, 2006) to the vector whose components are subvectors of the truncated K-L expansions. Also based on the Gaussian assumption, Zhu et al. (2016) introduced a Bayesian approach for estimating the functional graphical model. To overcome the limitation of the Gaussian assumption, Li and Solea (2018) developed a nonparametric functional graphical model based on Additive Conditional Independence (ACI), a three-way relation introduced by Li et al. (2014). This method amounts to performing sparse estimation of the precision matrix at the operator level: each entry of the matrix is an operator rather than a number, which can characterize ACI without the Gaussian assumption. Solea and Li (2022) introduced the functional copula Gaussian graphical model, which extends the copula Gaussian graphical model to functional data by transforming the scores of the KL expansions of X^1, \dots, X^p .

In this paper, we propose a nonparametric functional graphical model based on the recently developed nonlinear sufficient dimension reduction (SDR) for functional data (Li and Song, 2017), extending a recent work on sufficient graphical model scalar-valued random variables (Li and Kim, 2024). As already mentioned, construction of the functional graphical model hinges on evaluating the conditional independence relations $X^i \perp\!\!\!\perp X^j | X^{-(i,j)}$ for each pair $(i, j) \in V \times V$ with $i < j$. However, the high dimension of $X^{-(i,j)}$ hinders the accuracy in

assessing the conditional independence due to the curse of dimensionality (Bellman, 1961). Our idea is to first perform functional nonlinear SDR on $X^{-(i,j)}$, treating (X^i, X^j) as the response. The result is a low-dimensional random vector – the sufficient predictor U^{ij} – that satisfies

$$(X^i, X^j) \perp\!\!\!\perp X^{-(i,j)} | U^{ij}.$$

We then evaluate the conditional independence $X^i \perp\!\!\!\perp X^j | U^{ij}$ with the low-dimensional U^{ij} to determine the edge set of the graph. Compared with the additive functional graphical model of Li and Solea (2018), the present approach does not rely on additivity, and retains conditional independence as the graph construction criterion. Compared with the functional Gaussian graphical model of Qiao et al. (2019) and the copula functional graphical model of Solea and Li (2022), the present approach avoids the parametric or semiparametric model assumptions while maintaining a high estimation accuracy via SDR. Since our method combines the functional graphical model with SDR, we call it the functional sufficient graphical model (f-SGM).

The rest of the article is organized as follows. In Section 2 we rigorously define the f-SGM, and layout the two key steps for constructing it: functional SDR and determining conditional independence. In Sections 3 and 4, we describe how to implement these two steps at the population level. In section 5, we develop algorithms to implement the two steps at the sample level. In Section 6, we conduct simulation studies to evaluate our estimator and compare it with the existing methods. In Section 7, we apply our new estimator to an f-MRI dataset. We conclude with some discussion in Section 8.

2 Functional sufficient graphical models

In this section we rigorously define f-SGM at the population level. Since the structure is an extension of the sufficient graphical model introduced by Li and Kim (2024) for scalar-valued node variables, some of the theoretical results can be proved similarly as Li and Kim (2024). To make a distinction between the functional SGM and the SGM in Li and Kim (2024), we refer to the latter as the *multivariate* SGM.

Let (Ω, \mathcal{F}, P) be a probability space, and $\mathcal{H}_1, \dots, \mathcal{H}_p$ separable Hilbert spaces of functions defined on an interval $I \subseteq \mathbb{R}$, which represents time. Let $\mathcal{H} = \bigoplus_{i=1}^p \mathcal{H}_i$ be the direct sum of $\mathcal{H}_1, \dots, \mathcal{H}_p$. That is, \mathcal{H} is the Cartesian product $\mathcal{H}_1 \times \dots \times \mathcal{H}_p$ endowed with the inner product

$$\langle f, g \rangle_{\mathcal{H}} = \langle f_1, g_1 \rangle_{\mathcal{H}_1} + \dots + \langle f_p, g_p \rangle_{\mathcal{H}_p},$$

where $f = (f_1, \dots, f_p)$ and $g = (g_1, \dots, g_p)$ are members of \mathcal{H} . Let $X : \Omega \rightarrow \mathcal{H}$ be a random element in \mathcal{H} , measurable with respect to $\mathcal{F}/\mathcal{B}(\mathcal{H})$, $\mathcal{B}(\mathcal{H})$ being the Borel σ -field on \mathcal{H} . Then, $X = (X^1, \dots, X^p)$, where X^i is an random element in \mathcal{H}_i .

We assume that X follows a statistical graphical model with respect to \mathcal{G} in the sense that

$$X^i \perp\!\!\!\perp X^j | X^{-(i,j)} \Leftrightarrow (i, j) \notin \mathcal{E},$$

where $X^{-(i,j)}$ represents $(p-2)$ -dimensional subvector $\{X^k : k \notin \{i, j\}\}$ of X . For future exposition, we abbreviate the subvector (X^i, X^j) as $X^{(i,j)}$. Suppose we observe an i.i.d.

sample X_1, \dots, X_n of X . Our goal is to estimate the graph structure G based on the sample X_1, \dots, X_n .

For a generic random element S , let $\sigma(S)$ denote the σ -field generated by S . Here, following Billingsley (2008), we use the term “random element” S to refer to any measurable mapping from Ω to another measurable space $(\Omega_S, \mathcal{F}_S)$. So S can be a random variable in \mathbb{R} , a random vector in \mathbb{R}^k , a random function in a Hilbert space, or a vector or random functions in a direct sum of Hilbert spaces (which is our current setting). Suppose that for each $(i, j) \in V$, there is a sub- σ field $\mathcal{F}^{-(i,j)}$ of $\sigma(X^{-(i,j)})$ such that

$$X^{(i,j)} \perp\!\!\!\perp X^{-(i,j)} | \mathcal{F}^{-(i,j)}.$$

The problem of finding $\mathcal{F}^{-(i,j)}$ is called nonlinear SDR (Lee et al., 2013). Following Lee et al. (2013), we call $\mathcal{F}^{-(i,j)}$ a sufficient σ -field in $\sigma(X^{-(i,j)})$ for predicting $X^{(i,j)}$. As shown in Lee et al. (2013), under a mild condition, the intersection of all such sub σ -fields is still a sufficient σ -field. In that case, the intersection is called the central σ -field for $X^{(i,j)} | X^{-(i,j)}$. Throughout the rest of the paper, we assume the mild condition is satisfied, and the central σ -field always exists. For convenience, we reset the symbol $\mathcal{F}^{-(i,j)}$ to denote the central σ -field for $X^{(i,j)} | X^{-(i,j)}$.

Theorem 1 *If $\mathcal{F}^{-(i,j)}$ is the central σ -field for $X^{(i,j)} | X^{-(i,j)}$ for each $(i, j) \in V$, then*

$$X^i \perp\!\!\!\perp X^j | X^{-(i,j)} \Leftrightarrow X^i \perp\!\!\!\perp X^j | \mathcal{F}^{-(i,j)}.$$

This theorem is essentially the same as Theorem 1 of Li and Kim (2024), except that the random elements now take values in Hilbert spaces rather than in the real line. This motivates the following definition of f-SGM.

Definition 2 *A random element X in $\bigoplus_{i=1}^p \mathcal{H}_i$ is said to follow a f-SGM with respect to a graph G iff*

$$(i, j) \notin E \Leftrightarrow X^i \perp\!\!\!\perp X^j | \mathcal{F}^{-(i,j)}.$$

We write the statement “ X follows f-SGM with respect to a graph G ” as $X \sim \text{f-SGM}(G)$.

We estimate f-SGM(G) in the following two steps:

- (1) nonlinear functional SDR: find the central subspace $\mathcal{F}^{-(i,j)}$ by a nonlinear SDR method, such as the functional generalized sliced inverse regression (f-GSIR: Li and Song, 2017);
- (2) conditional independence thresholding: once we found the central σ -fields $\mathcal{F}^{-(i,j)}$, we develop a criterion to evaluate the conditional independence $X^i \perp\!\!\!\perp X^j | \mathcal{F}^{-(i,j)}$ by thresholding the norm of a linear operator that describes conditional dependence.

The first step largely resembles the first step of the multivariate SGM of Li and Kim (2024); whereas for the second step we will encounter an issue that is novel: we will be dealing with the mixture of a Hilbert space and a Euclidean space when we construct a linear operator for evaluating functional conditional independence. The next two sections will describe these two steps at the population level.

3 Functional nonlinear sufficient dimension reduction

We use the f-GSIR in Li and Song (2017) to perform the first step, the functional nonlinear SDR for $X^{(i,j)}$ versus $X^{-(i,j)}$. f-GSIR is based on a reproducing kernel Hilbert spaces (RKHS). For a pair of nodes $(i,j) \in V$, let

$$\mathcal{H}_{(i,j)} = \mathcal{H}_i \oplus \mathcal{H}_j, \quad \mathcal{H}_{-(i,j)} = \bigoplus_{k \notin \{i,j\}} \mathcal{H}_k.$$

Let $\kappa_{(i,j)} : \mathcal{H}_{(i,j)} \times \mathcal{H}_{(i,j)} \rightarrow \mathbb{R}$ be a positive kernel based on the inner product in $\mathcal{H}_{(i,j)}$. That is, there is a function $\rho : \mathbb{R}^3 \rightarrow \mathbb{R}$ such that, for $f, g \in \mathcal{H}_{(i,j)}$,

$$\kappa_{(i,j)}(f, g) = \rho(\langle f, f \rangle_{\mathcal{H}_{(i,j)}}, \langle f, g \rangle_{\mathcal{H}_{(i,j)}}, \langle g, g \rangle_{\mathcal{H}_{(i,j)}}).$$

Li and Song (2017) refers to such kernels as nested kernels in $\mathcal{H}_{(i,j)}$. For example, the Gaussian kernel and Laplacian radial basis functions,

$$\kappa_{(i,j)} = \exp(-\gamma \|f - g\|_{\mathcal{H}_{(i,j)}}^2), \quad \kappa_{(i,j)} = \exp(-\gamma \|f - g\|_{\mathcal{H}_{-(i,j)}}),$$

are nested kernels in $\mathcal{H}_{(i,j)}$. Let $\mathfrak{M}_{(i,j)}^{(0)}$ be the RKHS generated by $\kappa_{(i,j)}$. Similarly, let $\kappa_{-(i,j)}$ be a nested kernel defined on $\mathcal{H}_{-(i,j)} \times \mathcal{H}_{-(i,j)}$, and let $\mathfrak{M}_{-(i,j)}^{(0)}$ be the RKHS generated by $\kappa_{-(i,j)}$. Let $\mathfrak{S}_{-(i,j)}$ be the subset of $\mathfrak{M}_{-(i,j)}^{(0)}$ whose members are measurable with respect to $\mathcal{F}^{-(i,j)}$. This set of functions is called the central class functional nonlinear SDR of $X^{(i,j)}$ versus $X^{-(i,j)}$.

Let $\mu_{X^{(i,j)}}$ be the mean element in $\mathfrak{M}_{(i,j)}^{(0)}$, which is the member of $\mathfrak{M}_{(i,j)}^{(0)}$ defined as function $f \mapsto E\kappa_{(i,j)}(f, X)$. Let $\Sigma_{X^{(i,j)} X^{(i,j)}}$ be the covariance operator in $\mathfrak{M}_{(i,j)}^{(0)}$ defined as

$$E[(\kappa_{(i,j)}(\cdot, X) - \mu_{X^{(i,j)}}) \otimes (\kappa_{(i,j)}(\cdot, X) - \mu_{X^{(i,j)}})], \quad (2)$$

where \otimes is the tensor product. Here, $(\kappa_{(i,j)}(\cdot, X) - \mu_{X^{(i,j)}}) \otimes (\kappa_{(i,j)}(\cdot, X) - \mu_{X^{(i,j)}})$ is a random linear operator from $\mathfrak{M}_{(i,j)}^{(0)}$ to $\mathfrak{M}_{(i,j)}^{(0)}$, and the expectation of a random linear operator is defined via Riesz representation. See, for example, Li (2018) for more details. Similarly, we can define $\Sigma_{X^{-(i,j)} X^{-(i,j)}}$ is the covariance operator from $\mathfrak{M}_{-(i,j)}^{(0)}$ to $\mathfrak{M}_{-(i,j)}^{(0)}$:

$$E[(\kappa_{-(i,j)}(\cdot, X) - \mu_{X^{-(i,j)}}) \otimes (\kappa_{-(i,j)}(\cdot, X) - \mu_{X^{-(i,j)}})], \quad (3)$$

and $\Sigma_{X^{-(i,j)} X^{(i,j)}}$ is the cross covariance operator from $\mathfrak{M}_{(i,j)}^{(0)}$ to $\mathfrak{M}_{-(i,j)}^{(0)}$:

$$E[(\kappa_{-(i,j)}(\cdot, X) - \mu_{X^{-(i,j)}}) \otimes (\kappa_{(i,j)}(\cdot, X) - \mu_{X^{(i,j)}})]. \quad (4)$$

For a linear operator A from a Hilbert space \mathcal{H} to another Hilbert space \mathcal{H}' , let $\text{ran}(A) = \{Ah : h \in \mathcal{H}\}$ be the range of A , $\text{dom}(A)$ the domain of A , $\ker(A) = \{h \in \mathcal{H} : Ah = 0\}$ the kernel (or null space) of A , and $\overline{\text{ran}}(A)$ be the closure of $\text{ran}(A)$. Suppose $A : \mathcal{H} \rightarrow \mathcal{H}'$ is a self-adjoint operator with $\ker(A) = \{0\}$. Then A is an injection into \mathcal{H} , and we refer to the mapping $A^\dagger : \text{ran}(A) \rightarrow \overline{\text{ran}}(A)$ that maps a member h of $\text{ran}(A)$ to the unique member g of $\overline{\text{ran}}(A)$ such that $Ag = h$ as the Moore-Penrose inverse (see, for example, Li, 2018). Since $\text{dom}(A^\dagger) = \text{ran}(A)$, if $B : \mathcal{H}' \rightarrow \mathcal{H}$ is linear operator that maps into $\text{ran}(A)$, that is, $\text{ran}(B) \subseteq \text{ran}(A)$, then $A^\dagger B$ is a well defined operator from \mathcal{H}' to \mathcal{H} . The regression operator, which is the key to f-GSIR, is this form with $A = \Sigma_{X^{-(i,j)} X^{-(i,j)}}$ and $B = \Sigma_{X^{-(i,j)} X^{(i,j)}}$. Thus, for this operator to be defined, we need the following assumption.

Assumption 1 $\ker(\Sigma_{X^{-(i,j)}X^{-(i,j)}}) = \{0\}; \quad \text{ran}(\Sigma_{X^{-(i,j)}X^{(i,j)}}) \subseteq \text{ran}(\Sigma_{X^{-(i,j)}X^{-(i,j)}}).$

The first condition can be made without loss of generality. Indeed, if we let $\mathfrak{M}_{-(i,j)} = \overline{\text{ran}}(\Sigma_{X^{-(i,j)}X^{-(i,j)}})$, then $\Sigma_{X^{-(i,j)}X^{-(i,j)}}$, as a mapping from $\mathfrak{M}_{-(i,j)}$ to $\mathfrak{M}_{-(i,j)}$, indeed satisfies $\ker(\mathfrak{M}_{-(i,j)}) = \{0\}$. Since the orthogonal complement of $\overline{\text{ran}}(\Sigma_{X^{-(i,j)}X^{-(i,j)}})$ is $\ker(\Sigma_{X^{-(i,j)}X^{-(i,j)}})$, which only contains nonrandom element, replacing $\mathfrak{M}_{-(i,j)}^{(0)}$ by $\mathfrak{M}_{-(i,j)}$ does not lose generality as constants (i.e. nonrandom functions) play no role in determining conditional independence. For the same reason, we let $\text{dom}(\Sigma_{X^{(i,j)}X^{(i,j)}}) = \overline{\text{ran}}(\Sigma_{X^{(i,j)}X^{(i,j)}})$. As shown in Li and Song (2017),

$$\begin{aligned}\overline{\text{ran}}(\Sigma_{X^{-(i,j)}X^{-(i,j)}}) &= \overline{\text{span}}\{\kappa_{-(i,j)}(\cdot, X^{-(i,j)}) - \mu_{X^{-(i,j)}}\}, \\ \overline{\text{ran}}(\Sigma_{X^{(i,j)}X^{(i,j)}}) &= \overline{\text{span}}\{\kappa_{(i,j)}(\cdot, X^{(i,j)}) - \mu_{X^{(i,j)}}\}.\end{aligned}$$

The second condition in Assumption 1 is actually a kind of smoothness condition. For the intuitions and justification of this assumption, see, for example, Li and Song (2017) and Li (2018). Under Assumption 1, the mapping

$$R_{X^{-(i,j)}X^{(i,j)}} = \Sigma_{X^{-(i,j)}X^{-(i,j)}}^\dagger \Sigma_{X^{-(i,j)}X^{(i,j)}}$$

is a well defined operator from $\mathfrak{M}_{(i,j)}$ to $\mathfrak{M}_{-(i,j)}$ and we call it the regression operator. This regression operator provides a direct construction of the central subspace $\mathcal{F}^{-(i,j)}$ under the following assumption.

Assumption 2

- (1) $R_{X^{-(i,j)}X^{(i,j)}}$ is a finite-rank operator of rank d_{ij} ;
- (2) $\mathfrak{M}_{-(i,j)}$ is dense in $L_2(P_{X^{-(i,j)}})$ modulo constants, where $P_{X^{-(i,j)}}$ is the distribution of $X^{-(i,j)}$;
- (3) $\mathcal{F}^{-(i,j)}$ is complete.

It can be shown that, under Assumptions 1 and 2,

$$\sigma(\text{ran}(R_{X^{-(i,j)}X^{(i,j)}})) = \mathcal{F}^{-(i,j)}$$

See, Li and Song (2017) and Li (2018). Any estimator of $\mathcal{F}^{-(i,j)}$ that targets $\text{ran}(R_{X^{-(i,j)}X^{(i,j)}})$ is called f-GSIR. Let $A : \mathfrak{M}_{(i,j)} \rightarrow \mathfrak{M}_{(i,j)}$ be any nonsingular bounded linear operator. Estimating the range of $R_{X^{-(i,j)}X^{(i,j)}}$ is equivalent to solving the following optimization problem: at the k -th step,

$$\begin{aligned}\text{maximize} \quad & \langle f, R_{X^{-(i,j)}X^{(i,j)}} A R_{X^{(i,j)}X^{-(i,j)}} f \rangle_{\mathfrak{M}_{-(i,j)}} \\ \text{subject to} \quad & \begin{cases} \langle f, \Sigma_{X^{-(i,j)}X^{-(i,j)}} f \rangle_{\mathfrak{M}_{-(i,j)}} = 1 \\ \langle f, \Sigma_{X^{-(i,j)}X^{-(i,j)}} f_r \rangle_{\mathfrak{M}_{-(i,j)}} = 0, \quad r = 1, \dots, k-1 \end{cases}\end{aligned}\tag{5}$$

where f_1, \dots, f_{k-1} are the first $k-1$ solutions of the optimization problem. This problem is the eigen decomposition of the linear operator $R_{X^{-(i,j)}X^{(i,j)}} A R_{X^{(i,j)}X^{-(i,j)}}$. We follow Li and Song (2017) to take $A = \Sigma_{X^{(i,j)}X^{(i,j)}}^2$, and the linear operator in (5) reduces to

$\Sigma_{X^{-(i,j)}X^{(i,j)}}\Sigma_{X^{(i,j)}X^{-(i,j)}}$. The first d_{ij} eigenfunctions from the objective operator generates the central σ -field $\mathcal{G}_{-(i,j)}$. We use U^{ij} to denote the d_{ij} -dimensional random vector $(f_1(X), \dots, f_{d_{ij}}(X))$. For convenience, we assume that U^{ij} is supported on $\mathbb{R}^{d_{ij}}$.

In passing, we make a few remarks about Assumption 2. The first assumption essentially requires that the central σ -field is generated by finite number of functions in $\mathfrak{M}_{-(i,j)}$. The second assumption is satisfied if $\kappa_{-(i,j)}$ is a universal kernel, such as the Gaussian or Laplace kernel. Completeness in condition (3) is introduced by Lee et al. (2013), and, as argued in that paper, is satisfied by many forms of nonparametric or semiparametric models. For further justifications of these conditions, see Lee et al. (2013), Li and Song (2017), and Li (2018).

4 Determining conditional independence

In the second step, we determine whether the conditional independence $X^i \perp\!\!\!\perp X^j | U^{ij}$ holds. For this purpose, we adapt the linear operator for conditional dependence introduced Fukumizu et al. (2008), which was called the “Conjoined Conditional Covariance Operator” (CCCO) in Li and Kim (2024), to the current setting.

Let $\Omega_{U^{ij}} \subseteq \mathbb{R}^d$ be the support of the random vector U^{ij} , $\lambda_{ij} : \Omega_{U^{ij}} \times \Omega_{U^{ij}} \rightarrow \mathbb{R}$ a positive kernel, and $\kappa_i : \mathcal{H}_i \times \mathcal{H}_i \rightarrow \mathbb{R}$ another positive kernel. Let $\mathfrak{M}_i^{(0)}$ and $\mathfrak{N}_{ij}^{(0)}$ be the RKHS’s generated by the kernels κ_i and λ_{ij} , respectively. Let $\mathfrak{N}_{i,ij}^{(0)} = \mathfrak{M}_i^{(0)} \otimes \mathfrak{N}_{ij}^{(0)}$ be the direct product of $\mathfrak{M}_i^{(0)}$ and $\mathfrak{N}_{ij}^{(0)}$. By definition, the direct product $\mathfrak{M}_i^{(0)} \otimes \mathfrak{N}_{ij}^{(0)}$ is the RKHS generated by the positive kernel $\lambda_{i,ij} = \kappa_i \times \lambda_{ij}$. Note that $\lambda_{i,ij}$ is a mapping from $(\mathcal{H}_i \times \Omega_{U^{ij}}) \times (\mathcal{H}_i \times \Omega_{U^{ij}})$ to \mathbb{R} . For example, if we use the Gaussian radial basis functions for κ_i and λ_{ij} , then $\lambda_{i,ij}$ is the kernel

$$\lambda_{i,ij}((f, u), (g, v)) = \exp(-\gamma_1 \|f - g\|_{\mathcal{H}_i}^2 + \gamma_2 \|u - v\|^2),$$

where f, g are members of \mathcal{H}_i , u, v are members of $\mathbb{R}^{d_{ij}}$, and $\|\cdot\|$ is the Euclidean norm. For convenience, let $V^{i,ij}$ denote the random element (X^i, U^{ij}) . Note that $V^{i,ij}$ is a hybrid random element, with X^i being a Hilbertian random function and U^{ij} being a Euclidean random vector. We can define $V^{j,ij}$ similarly. Let $\mu_{V^{i,ij}}$ and $\mu_{V^{j,ij}}$ be the mean elements of $V^{i,ij}$ and $V^{j,ij}$. Again, they are partly function and partly vector objects in $\mathcal{H}_i \times \Omega_{U^{ij}}$ and $\mathcal{H}_j \times \Omega_{U^{ij}}$, respectively.

Let

$$\begin{aligned} \Sigma_{V^{i,ij}V^{j,ij}} &= E[(\lambda_{i,ij}(\cdot, V^{i,ij}) - \mu_{V^{i,ij}}) \otimes (\lambda_{i,ij}(\cdot, V^{i,ij}) - \mu_{V^{i,ij}})], \\ \Sigma_{V^{i,ij}U^{ij}} &= E[(\lambda_{i,ij}(\cdot, V^{i,ij}) - \mu_{V^{i,ij}}) \otimes (\lambda_{ij}(\cdot, U^{ij}) - \mu_{U^{ij}})], \\ \Sigma_{U^{ij}V^{j,ij}} &= E[(\lambda_{ij}(\cdot, U^{ij}) - \mu_{U^{ij}}) \otimes (\lambda_{i,ij}(\cdot, V^{i,ij}) - \mu_{V^{i,ij}})], \\ \Sigma_{U^{ij}U^{ij}} &= E[(\lambda_{ij}(\cdot, U^{ij}) - \mu_{U^{ij}}) \otimes (\lambda_{ij}(\cdot, U^{ij}) - \mu_{U^{ij}})]. \end{aligned} \tag{6}$$

Motivated by the same reason, we define the centered versions of $\mathfrak{N}_{i,ij}^{(0)}$ and $\mathfrak{N}_{ij}^{(0)}$ as $\mathfrak{N}_{i,ij} = \overline{\text{ran}}(\Sigma_{V^{i,ij}V^{j,ij}})$ and $\mathfrak{N}_{ij} = \overline{\text{ran}}(\Sigma_{U^{ij}U^{ij}})$, respectively. We make the following assumption.

Assumption 3 $\text{ran}(\Sigma_{U^{ij}V^{j,ij}}) \subseteq \text{ran}(\Sigma_{U^{ij}U^{ij}})$.

Under this assumption, the following operator is well defined:

$$\Sigma_{V^{i,ij}V^{j,ij}} - \Sigma_{V^{i,ij}U^{ij}} \Sigma_{U^{ij}U^{ij}}^\dagger \Sigma_{U^{ij}V^{j,ij}}.$$

This is the CCCO, and is denoted by $\Sigma_{\tilde{X}^i \tilde{X}^j|U^{ij}}$. To reflect the hybrid nature of the Hilbert spaces involved— X^i resides in the Hilbert space \mathcal{H}_i and U^{ij} resides in the Euclidean space $\mathbb{R}^{d_{ij}}$ —we use the term hybrid CCCO to refer to this version of the operator. Under the following assumption (Fukumizu et al., 2008), the hybrid CCCO characterizes conditional independence.

Assumption 4

- (1) the kernels $\lambda_{i,ij}$ and $\lambda_{j,ij}$ are universal;
- (2) the space \mathfrak{N}_{ij} is dense in $L_2(P_{U^{ij}})$ modula constants;
- (3) the condition $E[\kappa(W,W)] < \infty$ holds for

$$\begin{cases} \kappa = \lambda_{i,ij} \\ W = (X^i, U^{ij}) \end{cases}, \quad \begin{cases} \kappa = \lambda_{j,ij} \\ W = (X^j, U^{ij}) \end{cases}, \quad \begin{cases} \kappa = \lambda_{ij} \\ W = U^{ij} \end{cases}.$$

Theorem 3 *Under Assumption 4,*

$$(i,j) \notin \mathsf{E} \Leftrightarrow X^i \perp\!\!\!\perp X^j | U^{ij} \Leftrightarrow \Sigma_{\tilde{X}^i \tilde{X}^j|U^{ij}} = 0.$$

The proof of the theorem is similar to that of Corollary 5 in Li and Kim (2024), and is omitted. The theorem suggests that we can threshold the norm of the sample estimate of the hybrid CCCO to estimate the graph G .

5 Sample-level implementation of f-SGM

5.1 Coordinate mapping

Our algorithms are best presented by a systematic use of the coordinate notation that represents members of a Hilbert space and linear operators between Hilbert spaces as vectors and matrices (see, for example, Horn and Johnson, 2012 and Li, 2018). Let $\mathcal{H}_1, \mathcal{H}_2, \mathcal{H}_3$ be finite-dimensional Hilbert spaces of dimensions n_1, n_2 , and n_3 , and let $\mathcal{B}_1, \mathcal{B}_2$, and \mathcal{B}_3 be the bases of $\mathcal{H}_1, \mathcal{H}_2$, and \mathcal{H}_3 , respectively. For $r = 1, 2, 3$, let $\mathcal{B}_r = \{b_{r1}, \dots, b_{rn_r}\}$. Any member f , say, of \mathcal{H}_1 , can be represented as $\alpha_1 b_{11} + \dots + \alpha_{n_1} b_{1n_1}$. The vector $(\alpha_1, \dots, \alpha_{n_1})^\top$ is called the coordinate of f with respect to \mathcal{B}_1 , and is written as $[f]_{\mathcal{B}_1}$. If $A_1 : \mathcal{H}_1 \rightarrow \mathcal{H}_2$ is a linear operator and f is a member of \mathcal{H}_1 , then the coordinate $[Af]_{\mathcal{B}_2}$ can be represented as $C[f]_{\mathcal{B}_1}$, where C is the $n_2 \times n_1$ matrix $([A_1 b_{11}]_{\mathcal{B}_2}, \dots, [A_1 b_{1n_1}]_{\mathcal{B}_2})$. This matrix is called the coordinate of A_1 with respect to $(\mathcal{B}_1, \mathcal{B}_2)$, and is written as $\mathcal{B}_2[A_1]_{\mathcal{B}_1}$. Furthermore, if $A_2 : \mathcal{H}_2 \rightarrow \mathcal{H}_3$ is a linear operator, then, $\mathcal{B}_3[A_2 A_1]_{\mathcal{B}_1} = (\mathcal{B}_3[A_2]_{\mathcal{B}_2})(\mathcal{B}_2[A_1]_{\mathcal{B}_1})$. The mappings such as $f \mapsto [f]_{\mathcal{B}_1}$ and $A_1 \mapsto_{\mathcal{B}_2} [A_1]_{\mathcal{B}_1}$ are called coordinate mappings. For further properties of these mappings, see Li and Solea (2018), Li (2018), and Solea and Li (2022).

5.2 First-level Hilbert spaces

We now construct the first-level Hilbert spaces $\mathcal{H}_1, \dots, \mathcal{H}_p$ based on a sample of observations on the multivariate functional data. There are more than one ways to construct these spaces — for example, using spline spaces or RKHS. Here, as in Li and

Song (2017) and Solea and Li (2022), we use the RKHS. Let X_1, \dots, X_n be an i.i.d. sample of X and, for each X_a , let X_a^1, \dots, X_a^p be the p -components of X_a . In practice, we do not observe the entire function $\{X_a(t) : t \in I\}$, but instead only observe it on a finite set of time points, say $J_a = \{t_{a1}, \dots, t_{ama}\}$, where $t_{a1} < \dots < t_{ama}$. Let $J = \bigcup_{a=1}^n J_a$ be the collection of all time points on which at least one of X_1, \dots, X_n is observed, and represent this union by $\{u_1, \dots, u_N\}$, where $u_1 < \dots < u_N$ are distinct members of $\{t_{ab} : b = 1, \dots, m_a, a = 1, \dots, n\}$. Note that $N \leq \sum_{a=1}^n m_a$. Let $\tau : I \times I \rightarrow \mathbb{R}$ be a positive kernel. We set

$$\mathcal{H}_1 = \dots = \mathcal{H}_p = \text{span}\{\tau(\cdot, u_c) : c = 1, \dots, N\}.$$

We next represent the functional data X_1^i, \dots, X_n^i as members of \mathcal{H}_i . Let $S_a \subseteq \{1, \dots, N\}$ be the set of indices for members of J_a ; that is, $\{u_c : c \in S_a\} = \{t_{a1}, \dots, t_{ama}\}$. Let $\mathcal{B}_T = \{\tau(\cdot, u_c) : c = 1, \dots, N\}$ be the basis of \mathcal{H}_i . Since $X_a^i(t)$ is observed only for $t \in J_a$, we use the functions in the set $\{\tau(\cdot, u_c) : c \in S_a\}$ to approximate X_a^i .

To make this clear, let us introduce more notations. For a vector $v = (v_1, \dots, v_N)^\top$ in \mathbb{R}^N and a subset A of $\{1, \dots, N\}$, let $v(A)$ denote the subvector $\{v_c : c \in A\}$. For a function $h : \mathbb{R} \rightarrow \mathbb{R}$, and a vector $w = (w_1, \dots, w_r)^\top \in \mathbb{R}^r$, let $h(w)$ represent the vector $(h(w_1), \dots, h(w_r))^\top$. For a function $k : \mathbb{R} \times \mathbb{R} \rightarrow \mathbb{R}$, and the w just defined, let $k(w, w)$ represent the $r \times r$ matrix $\{k(w_a, w_b) : a, b = 1, \dots, r\}$, and let $k(\cdot, w)$ represent the r -dimensional function $(k(\cdot, w_1), \dots, k(\cdot, w_r))^\top$.

Using the functions in $\{\tau(\cdot, u_c) : c \in S_a\}$ to approximate X_a^i amounts to assuming the subvector $[X_a^i]_{\mathcal{B}_T}(S_a^c) = 0$ and only using the subvector $[X_a^i]_{\mathcal{B}_T}(S_a)$. For any $t \in I$, we have $X_a^i(t) = \{[X_a^i]_{\mathcal{B}_T}(S_a)\}^\top \tau(t, u(S_a))$. Evaluating this equation at $t \in J_a$, we have

$$X_a^i(u(S_a)) = \begin{pmatrix} \tau(t_{a1}, u(S_a))^\top \\ \vdots \\ \tau(t_{ama}, u(S_a))^\top \end{pmatrix} [X_a^i]_{\mathcal{B}_T}(S_a) = \tau(u(S_a), u(S_a)) [X_a^i]_{\mathcal{B}_T}(S_a).$$

Solving the above equation with Tychonoff regularization, we have

$$[X_a^i]_{\mathcal{B}_T}(S_a) = \{\tau(u(S_a), u(S_a)) + \eta_n I_{m_a}\}^{-1} X_a^i(u(S_a)). \quad (7)$$

So, the coordinate of X_a^i with respect to \mathcal{B}_T is specified by the above equation and $[X_a^i]_{\mathcal{B}_T}(S_a^c) = 0$. Note that our construction works for both the balanced case, where all the J_a 's are the same, and the unbalanced case, where they are different.

5.3 Second-level Hilbert spaces

Let us now turn to the second-level RKHS's: $\mathfrak{M}_{(i,j)}$ and $\mathfrak{M}_{-(i,j)}$ for each $(i, j) \in \mathbb{V}$. Mimicking the population-level construction, let $\mathfrak{M}_{(i,j)}$ and $\mathfrak{M}_{-(i,j)}$ be the centered RKHS's spanned by the sets

$$\begin{aligned} \mathfrak{B}_{(i,j)} &= \{\kappa_{(i,j)}(\cdot, X_a^{(i,j)}) - \hat{\mu}_{X^{(i,j)}} : a = 1, \dots, n\}, \\ \mathfrak{B}_{-(i,j)} &= \{\kappa_{-(i,j)}(\cdot, X_a^{(i,j)}) - \hat{\mu}_{X^{-(i,j)}} : a = 1, \dots, n\}, \end{aligned}$$

where $\hat{\mu}_{X^{(i,j)}}$ and $\hat{\mu}_{X^{-(i,j)}}$ are the functions $E_n \kappa_{(i,j)}(\cdot, X^{(i,j)})$ and $E_n \kappa_{-(i,j)}(\cdot, X^{-(i,j)})$. The inner products of $\mathfrak{M}_{(i,j)}$ and $\mathfrak{M}_{-(i,j)}$ are determined by $\kappa_{(i,j)}$ and $\kappa_{-(i,j)}$, respectively.

5.4 f-GSIR

We estimate $\Sigma_{X^{-(i,j)}X^{-(i,j)}}$, $\Sigma_{X^{(i,j)}X^{(i,j)}}$, and $\Sigma_{X^{(i,j)}X^{-(i,j)}}$ by replacing every expectation E and (2), (3), and (4) by the sample average E_n , including the expectations for the mean elements, by sample averages. Denote the resulting estimates by $\hat{\Sigma}_{X^{-(i,j)}X^{-(i,j)}}$, $\hat{\Sigma}_{X^{(i,j)}X^{(i,j)}}$, and $\hat{\Sigma}_{X^{(i,j)}X^{-(i,j)}}$. Let $K_{(i,j)}$ be the $n \times n$ Gram matrix $\{\kappa_{-(i,j)}(X_a^{-(i,j)}, X_b^{-(i,j)}) : a, b = 1, \dots, n\}$, and let $K_{-(i,j)}$ be similarly defined. Let $Q_n = I_n - 1_n 1_n^\top/n$ be the projection onto the orthogonal complement of the vector $1_n = (1, \dots, 1)^\top$ in \mathbb{R}^n . Let $G_{(i,j)}$ and $G_{-(i,j)}$ be the centered Gram matrices $Q_n K_{(i,j)} Q_n$ and $Q_n K_{-(i,j)} Q_n$. It can be shown that the coordinates of $\hat{\Sigma}_{X^{-(i,j)}X^{-(i,j)}}$, $\hat{\Sigma}_{X^{(i,j)}X^{(i,j)}}$, and $\hat{\Sigma}_{X^{(i,j)}X^{-(i,j)}}$ are, respectively

$$\begin{aligned} \mathcal{B}_{-(i,j)}[\hat{\Sigma}_{X^{-(i,j)}X^{-(i,j)}}]_{\mathcal{B}_{-(i,j)}} &= n^{-1}G_{-(i,j)}, \\ \mathcal{B}_{(i,j)}[\hat{\Sigma}_{X^{(i,j)}X^{(i,j)}}]_{\mathcal{B}_{(i,j)}} &= n^{-1}G_{(i,j)}, \\ \mathcal{B}_{(i,j)}[\hat{\Sigma}_{X^{(i,j)}X^{-(i,j)}}]_{\mathcal{B}_{-(i,j)}} &= n^{-1}G_{-(i,j)}. \end{aligned} \quad (8)$$

Moreover, for any $f_1, f_2 \in \mathfrak{M}_{-(i,j)}$ and $g_1, g_2 \in \mathfrak{M}_{(i,j)}$,

$$\langle f_1, f_2 \rangle_{\mathfrak{M}_{-(i,j)}} = ([f_1]_{\mathcal{B}_{-(i,j)}})G_{-(i,j)}([f_2]_{\mathcal{B}_{-(i,j)}}), \quad \langle g_1, g_2 \rangle_{\mathfrak{M}_{(i,j)}} = ([g_1]_{\mathcal{B}_{(i,j)}})G_{(i,j)}([g_2]_{\mathcal{B}_{(i,j)}}).$$

In this paper we take the operator $A : \mathfrak{M}_{(i,j)} \rightarrow \mathfrak{M}_{(i,j)}$ in (5) to be the identity mapping, whose coordinate with respect to $\mathfrak{M}_{(i,j)}$ is Q_n (see, for example, Solea and Li, 2022). Therefore, the sample version of the quadratic form in (5) is

$$\langle f, \hat{\Sigma}_{X^{-(i,j)}X^{(i,j)}} \hat{\Sigma}_{X^{(i,j)}X^{-(i,j)}} f \rangle_{\mathfrak{M}_{-(i,j)}} = ([f]_{\mathcal{B}_{-(i,j)}})G_{-(i,j)}G_{(i,j)}G_{-(i,j)}([f]_{\mathcal{B}_{-(i,j)}}),$$

and the sample version of the quadratic form in (5) with Tychonoff regularization is

$$\langle f, \hat{\Sigma}_{X^{-(i,j)}X^{-(i,j)}} f \rangle_{\mathfrak{M}_{-(i,j)}} = ([f]_{\mathcal{B}_{-(i,j)}})(G_{-(i,j)} + \epsilon_n^{ij}I_n)^2([f]_{\mathcal{B}_{-(i,j)}}). \quad (9)$$

To solve this generalized eigenvalue problem, we set $v = (G_{-(i,j)} + \epsilon_n I_n)([f]_{\mathcal{B}_{-(i,j)}})$, which implies $v = (G_{-(i,j)} + \epsilon_n^{ij}I_n)^{-1}([f]_{\mathcal{B}_{-(i,j)}})$. Then v is an eigenvector of the matrix

$$(G_{-(i,j)} + \epsilon_n^{ij}I_n)^{-1}G_{-(i,j)}G_{(i,j)}G_{-(i,j)}(G_{-(i,j)} + \epsilon_n^{ij}I_n)^{-1},$$

and the coordinate of the corresponding eigenfunction is $[f]_{\mathcal{B}_{-(i,j)}} = (G_{-(i,j)} + \epsilon_n^{ij}I_n)^{-1}v$. Let $\hat{f}_1, \dots, \hat{f}_{d_{ij}}$ be the first d_{ij} eigenfunctions defined by the coordinates

$$(G_{-(i,j)} + \epsilon_n^{ij}I_n)^{-1}v_1, \dots, (G_{-(i,j)} + \epsilon_n^{ij}I_n)^{-1}v_{d_{ij}}.$$

The estimated sufficient predictor U^{ij} is the d_{ij} -vector $(\hat{f}_1(X^{-(i,j)}), \dots, \hat{f}_{d_{ij}}(X^{-(i,j)}))^\top$.

5.5 Third-level Hilbert spaces

Having obtained the sufficient predictor U^{ij} , we now construct the third-level Hilbert spaces based on (X_a^i, X_a^j, U_a^{ij}) , $a = 1, \dots, n$. Mimicking the population-level construction, let $\mathfrak{N}_{i,ij}$, $\mathfrak{N}_{j,ij}$, and \mathfrak{N}_{ij} be the centered RKHS's spanned by the sets

$$\begin{aligned} \mathfrak{B}_{i,ij} &= \{\lambda_{i,ij}(\cdot, V_a^{i,ij}) - \hat{\mu}_{V^{i,ij}} : a = 1, \dots, n\}, \\ \mathfrak{B}_{j,ij} &= \{\lambda_{j,ij}(\cdot, V_a^{j,ij}) - \hat{\mu}_{V^{j,ij}} : a = 1, \dots, n\}, \\ \mathfrak{B}_{ij} &= \{\lambda_{ij}(\cdot, U_a^{ij}) - \hat{\mu}_{U^{ij}} : a = 1, \dots, n\}, \end{aligned}$$

where $\hat{\mu}_{V^{i,ij}}$, $\hat{\mu}_{V^{j,ij}}$, and $\hat{\mu}_{U^{ij}}$ are the mean elements $E_n \lambda_{i,ij}(\cdot, V^{i,ij})$, $E_n \lambda_{j,ij}(\cdot, V^{j,ij})$, and $E_n \lambda_{ij}(\cdot, U^{ij})$, respectively, their inner products determined by their respective kernels.

5.6 Hybrid CCCO and its HS-norm

We estimate the operators in (6) by replacing the expectation operator E therein with the sample average operator E_n , including the expectations in the mean elements. We denote these estimators by putting a hat on the symbols representing the four operators. We then estimate the hybrid CCCO by

$$\hat{\Sigma}_{\ddot{X}_i \ddot{X}_j | U^{ij}} = \hat{\Sigma}_{V^{i,ij} V^{j,ij}} - \hat{\Sigma}_{V^{i,ij} U^{ij}} (\hat{\Sigma}_{U^{ij} U^{ij}} + \delta_n^{ij} I)^{-1} \hat{\Sigma}_{U^{ij} V^{j,ij}}, \quad (10)$$

where $\delta_n^{ij} > 0$ is a tuning parameter. We estimate the graph G by thresholding the Hilbert-Schmidt norm of the hybrid CCCO for $(i, j) \notin V$.

The coordinate form of the above estimator is derived similarly as we did for f-GSIR. For each $(i, j) \in V$, let $L_{i,ij}$, $L_{j,ij}$, and L_{ij} be the $n \times n$ Gram matrices:

$$\{\lambda_{i,ij}(V_a^{i,ij}, V_b^{i,ij})\}_{a,b=1}^n, \quad \{\lambda_{j,ij}(V_a^{j,ij}, V_b^{j,ij})\}_{a,b=1}^n, \quad \{\lambda_{ij}(U_a^{ij}, U_b^{ij})\}_{a,b=1}^n,$$

respectively, and let $H_{i,ij} = Q_n L_{i,ij} Q_n$, $H_{j,ij} = Q_n L_{j,ij} Q_n$, and $H_{ij} = Q_n L_{ij} Q_n$. Similar to (8), we have

$$\begin{aligned} \mathfrak{B}_{i,ij} [\hat{\Sigma}_{V^{i,ij} V^{j,ij}}]_{\mathfrak{B}_{j,ij}} &= n^{-1} H_{j,ij}, & \mathfrak{B}_{i,ij} [\hat{\Sigma}_{V^{i,ij} U^{ij}}]_{\mathfrak{B}_{ij}} &= n^{-1} H_{ij} \\ \mathfrak{B}_{ij} [\hat{\Sigma}_{U^{ij} U^{ij}}]_{\mathfrak{B}_{ij}} &= n^{-1} H_{ij}, & \mathfrak{B}_{ij} [\hat{\Sigma}_{U^{ij} V^{j,ij}}]_{\mathfrak{B}_{j,ij}} &= n^{-1} H_{j,ij}. \end{aligned}$$

Therefore, by the rules of coordinating mapping described in Solea and Li (2022), we have

$$\mathfrak{B}_{i,ij} [\hat{\Sigma}_{\ddot{X}_i \ddot{X}_j | U^{ij}}]_{\mathfrak{B}_{j,ij}} = H_{j,ij} - H_{ij} (H_{ij} + \delta_n^{ij} I_n)^{-1} H_{j,ij}.$$

We assess conditional dependence between X^i and X^j given $X^{-(i,j)}$ by thresholding the Hilbert-Schmidt norm of $\hat{\Sigma}_{\ddot{X}_i \ddot{X}_j | U^{ij}}$. The Hilbert Schmidt norm of a finite-rank operator can be represented as the Frobenius norm of a matrix as follows. Let $\|\cdot\|_{\text{HS}}$ and $\|\cdot\|_{\text{TR}}$ denote the Hilbert-Schmidt norm and trace norm of an operator, respectively, and let $\|\cdot\|_{\text{F}}$ denote Frobenius norm of a matrix. Let $\mathfrak{M}_1, \mathfrak{M}_2$ be finite-dimensional Hilbert space with spanning systems \mathfrak{B}_1 and \mathfrak{B}_2 . Let G_1 and G_2 be the Gram matrices of \mathfrak{B}_1 and \mathfrak{B}_2 . Let $A : \mathfrak{M}_1 \rightarrow \mathfrak{M}_2$ be a linear operator. Then, $\|A\|_{\text{HS}}^2 = \|A^* A\|_{\text{TR}}$, where A^* is the adjoint operator of A . The eigenvalues of $A^* A$ are defined through the maximization problem:

$$\text{maximize } \langle f, A^* A f \rangle_{\mathfrak{M}_1} \quad \text{subject to } \langle f, f \rangle_{\mathfrak{M}_1}.$$

Reexpressed in coordinate representation, the above problem becomes

$$\text{maximize } ([f]_{\mathfrak{B}_1})^\top G_1 ([A^* A]_{\mathfrak{B}_1}) ([f]_{\mathfrak{B}_1}) \quad \text{subject to } ([f]_{\mathfrak{B}_1})^\top G_1 ([f]_{\mathfrak{B}_1}) = 1.$$

Thus we see that the eigenvalues of the operator $A^* A$ are the same as the eigenvalues of the matrix $G_1^{1/2} ([A^* A]_{\mathfrak{B}_1}) G_1^{\dagger 1/2}$, where $G_1^{\dagger 1/2}$ denotes $(G_1^\dagger)^{1/2}$, and G_1^\dagger denotes the Moore-Penrose inverse of G_1 . Consequently,

$$\|A^* A\|_{\text{TR}} = \text{tr}(G_1^{1/2} ([A^* A]_{\mathfrak{B}_1}) G_1^{\dagger 1/2}).$$

Furthermore, from $\langle A^* f, g \rangle_{\mathfrak{M}_1} = \langle f, A g \rangle_{\mathfrak{M}_2}$ for all $g \in \mathfrak{M}_1, f \in \mathfrak{M}_2$ we see that $(\mathfrak{B}_1[A^*]_{\mathfrak{B}_2})^\top G_1 = G_2(\mathfrak{B}_2[A]_{\mathfrak{B}_1})$, implying $\mathfrak{B}_1[A^*]_{\mathfrak{B}_2} = G_1^\dagger(\mathfrak{B}_2[A]_{\mathfrak{B}_1})^\top G_2$. Hence

$$\begin{aligned} \text{tr}\{G_1^{1/2}(\mathfrak{B}_1[A^*A]_{\mathfrak{B}_1})G_1^{\dagger 1/2}\} &= \text{tr}\{G_1^{\dagger 1/2}(\mathfrak{B}_2[A]_{\mathfrak{B}_1})^\top G_2(\mathfrak{B}_2[A]_{\mathfrak{B}_1})G_1^{\dagger 1/2}\} \\ &= \|G_2^{1/2}(\mathfrak{B}_2[A]_{\mathfrak{B}_1})G_1^{\dagger 1/2}\|_{\text{F}}^2. \end{aligned}$$

Thus we have proved

$$\|A\|_{\text{HS}} = \|G_2^{1/2}(\mathfrak{B}_2[A]_{\mathfrak{B}_1})G_1^{\dagger 1/2}\|_{\text{F}}. \quad (11)$$

This identity was used in Li and Kim (2024) without proof. By (11), we have

$$\|\hat{\Sigma}_{\ddot{X}_i \ddot{X}_j | U^{ij}}\|_{\text{HS}} = \|H_{i,ij}^{1/2}(H_{j,ij} - H_{ij}(H_{ij} + \delta_n^{ij} I_n)^{-1}H_{j,ij})H_{j,ij}^{\dagger 1/2}\|_{\text{F}}.$$

Estimation of the edge set is then based on thresholding this norm; that is,

$$\hat{E} = \{(i, j) \in V : \|\hat{\Sigma}_{\ddot{X}_i \ddot{X}_j | U^{ij}}\|_{\text{HS}} > \rho_n\} \quad (12)$$

for some chosen threshold $\rho_n > 0$.

5.7 Determination of tuning parameters

There are two types of tuning parameters: those that appears in the kernels and those for the Tychonoff regularization. For the kernels, we have the kernel τ for the first level Hilbert spaces; the kernels $\kappa_{(i,j)}$ and $\kappa_{-(i,j)}$ for the second-level Hilbert spaces; the kernels λ_{ij} , $\lambda_{i,ij} = \kappa_i \times \lambda_{ij}$, and $\lambda_{j,ij} = \kappa_j \times \lambda_{ij}$ for the third-level Hilbert spaces. In this paper we use the Brownian motion kernel for τ ; that is, $\tau(u_1, u_2) = \min(u_1, u_2)$ for $u_1, u_2 \in I$, which contains no tuning parameter. For the second- and third-level Hilbert spaces, we use the Gaussian radial basis function as the kernel. That is, suppose $\kappa : \mathcal{H} \times \mathcal{H} \rightarrow \mathbb{R}$ is a generic positive kernel, where \mathcal{H} can be a Euclidean space (as is the case for λ_{ij}) or an RKHS (as is the case for $\kappa_i, \kappa_j, \kappa_{(i,j)}, \kappa_{-(i,j)}$). For any $s_1, s_2 \in \mathcal{H}$, the Gaussian RBF is defined as

$$\kappa(s_1, s_2) = \exp(-\gamma \|s_1 - s_2\|^2),$$

where $\|\cdot\|$ is the norm in \mathcal{H} . If S_1, \dots, S_n are a sample of observations in \mathcal{H} , then γ is chosen by

$$\gamma = \frac{\binom{n}{2}^2}{\sum_{a < b} \|S_a - S_b\|_{\mathcal{H}}^2}.$$

There are three types of Tychonoff regularization parameters: η_n in (7), ϵ_n^{ij} in (9), and δ_n^{ij} in (10). We use generalized cross validation (GCV) to determine these parameters. For η_n , we minimize the function

$$\text{GCV}(\eta) = \sum_{i=1}^p \sum_{a=1}^n \frac{\|X_a^i(J_a) - K_T(J_a, J_a) \{K_T(J_a, J_a) + \eta I_{m_a}\}^{-1} X_a^i(J_a)\|_{\text{F}}^2}{m_a^{-1} \text{tr}\{I_{m_a} - K_T(J_a, J_a)(K_T(J_a, J_a) + \eta I_{m_a})^{-1}\}}.$$

For ϵ_n^{ij} , we first reparameterize it as $\epsilon \lambda_{\max}(G_{-(i,j)})$, where λ_{\max} represents the largest eigenvalue. The reason for doing so is to bring the scale of the tuning parameter to the range of eigenvalues of the matrix being regularized. We then minimize the function

$$\text{GCV}(\epsilon) = \sum_{i < j}^p \frac{\|G_{(i,j)} - G_{-(i,j)}\{G_{-(i,j)} + \epsilon \lambda_{\max}(G_{-(i,j)})I_n\}^{-1}G_{(i,j)}\|_{\text{F}}^2}{n^{-1}\text{tr}\{I_n - G_{-(i,j)}\{G_{-(i,j)} + \epsilon \lambda_{\max}(G_{-(i,j)})I_n\}^{-1}\}}.$$

For δ_n^{ij} , we first reparameterize it as $\delta \lambda_{\max}(G_{-(i,j)})$, and then minimize the function

$$\text{GCV}(\delta) = \sum_{i < j}^p \frac{\|G_{(i,j)} - H_{ij}\{H_{ij} + \delta \lambda_{\max}(H_{ij})I_n\}^{-1}G_{(i,j)}\|_{\text{F}}^2}{n^{-1}\text{tr}\{I_n - H_{ij}\{H_{ij} + \delta \lambda_{\max}(H_{ij})I_n\}^{-1}\}}.$$

The minimizations are carried out over grids of η , ϵ , and δ .

To determine the threshold ρ_n in (12), similar to Li and Kim (2024) and Lee et al. (2016a), we use GCV criterion to find an appropriate value of ρ which minimizes prediction error. Let $\hat{E}(\rho)$ be the estimated edges based on the threshold ρ and $\mathcal{N}^i(\rho) = \{j \in V | (i, j) \in \hat{E}(\rho)\}$ be the neighborhood of i -th node in the graph of $G = (V, \hat{E}(\rho))$. Then, we decide ρ using GCV as

$$\text{GCV}(\rho) = \sum_{i=1}^p \frac{\|G_{X^i} - G_{C^i(\rho)}^{\top} [G_{\mathcal{N}^i(\rho)} + \epsilon \lambda_{\max}(G_{\mathcal{N}^i(\rho)})I_n]^{-1}G_{X^i}\|_{\text{F}}^2}{\frac{1}{n}\text{tr}\{I_n - G_{\mathcal{N}^i(\rho)}^{\top} [G_{\mathcal{N}^i(\rho)} + \epsilon \lambda_{\max}(G_{\mathcal{N}^i(\rho)})I_n]^{-1}\}}, \quad (13)$$

where $G_{\mathcal{N}^i(\rho)}$ indicates a gram matrix from $X^{\mathcal{N}^i(\rho)}$. We can use GCV based on the grid $\rho \in \{k \times 10^{-2} | k = 1, \dots, 7\}$. The idea behind this method is applying GCV to residuals from the regression of the feature of each node X^i on the feature of its neighborhood nodes $X^{\mathcal{N}^i(\rho)}$.

6 Simulation comparisons with existing methods

In this section we compare our two-step f-SGM estimator with several existing estimators of the functional graphical model, including the functional Gaussian graphical model (FGGM) of Qiao et al. (2019), the nonparametric additive estimator based on the functional additive precision operator (FAPO) proposed in Li and Solea (2018). We also compare our method with the naive method of extracting the first functional principal component from the observations at each node and then feeding the vector of first principal components into the sufficient graphical model developed by Li and Kim (2024); we refer to this method as the naive sufficient graphical models (n-SGM).

For a comprehensive comparison, we include a broad spectrum of models that favor each of the above methods. In particular, Models I and II are nonlinear and additive models that favor FAPO, which is additive in nature. Model III contains heteroscedasticity that cannot be captured by either the Gaussian method or the additive method, but can be captured by our method. Model IV is the Gaussian model that favors FGGM. We then repeat models I, III, and IV to increase the dimension p . We generated undirected functional graphical models by first constructing structural equations, and then removing arrows and joining parents (if any). In all simulations, we use the Brownian motion covariance kernel

to construct the first-level Hilbert spaces, and use the Gaussian RBF for the second- and third-level Hilbert spaces. The tuning parameters are determined according to Section 5.7. The grids for η , ϵ , and δ for their minimization processes are taken to be $\{3 \times 10^b : b = 0, \dots, 5\}$. Because these Tychonoff regularization parameters are quite stable, we compute their average values for the first ten samples and use them for the rest of the simulation for each model.

6.1 Nonlinear models

$$\begin{aligned} \text{Model I: } X^{(1)}(t) &= \epsilon^{(1)}(t), & X^{(2)}(t) &= (0.5 + |X^{(1)}(t)|)^2 + \epsilon^{(2)}(t), \\ X^{(3)}(t) &= \epsilon^{(3)}(t), & X^{(4)}(t) &= \cos(\pi X^{(2)}(t)) + \epsilon^{(4)}(t), \\ X^{(5)}(t) &= 5(X^{(3)}(t))^2 + \epsilon^{(5)}(t). \end{aligned}$$

Here the random functions $\epsilon^{(i)}(t)$, $i = 1, 2, 3, 4, 5$, are generated as $\sum_{j=1}^{50} \xi_j \kappa_T(t, t_j)$, where ξ_1, \dots, ξ_{50} are i.i.d. $N(0, 1)$, t_1, \dots, t_{50} are i.i.d. $U(0, 1)$, and $\kappa_T(t, s) = \min(s, t)$ is the Brownian motion covariance kernel. We consider both balanced and unbalanced case. For the balanced case we pick equally spaced 10 points t_1, \dots, t_{10} from 0 to 1. For the unbalanced case we generate 100 samples in $U(0, 1)$ and pick t_1, \dots, t_{10} randomly from them.

Figure 2 shows the ROC curves of different methods for both balanced and unbalanced cases. The red lines indicate f-SGM, the blue lines indicate FAPO, red dashed lines indicate n-SGM, and the black line is for FGGM. We choose the sample sizes to be $n = 100, 200$ and repeat each simulation to find the averaged ROC curves. For FGGM, we use the first two functional principal components, because in most of the times, they explain over 90% of the total variation.

We observe that f-SGM and FAPO perform significantly better than the FGGM and n-SGM. The performance of f-SGM is very similar to FAPO, which is significant considering this is an additive model that favors FAPO.

Time	n	n-SGM	FAPO	f-SGM	FGGM
Balanced	100	0.65(0.06)	0.98(0.01)	0.97(0.01)	0.52(0.17)
	200	0.63(0.06)	0.98(0.01)	0.97(0.01)	0.53(0.12)
Unbalanced	100	0.80(0.06)	0.98(0.01)	0.97(0.01)	0.57(0.15)
	200	0.82(0.05)	0.98(0.01)	0.97(0.01)	0.57(0.14)

Table 1: AUC results for model I.

Model II. This is again a nonlinear additive model, but with more complex features than Model I:

$$\begin{aligned} X^{(1)}(t) &= \epsilon^{(1)}(t), & X^{(2)}(t) &= \epsilon^{(2)}(t), & X^{(3)}(t) &= \exp(X^{(1)}(t)) + \epsilon^{(3)}(t), \\ X^{(4)}(t) &= \epsilon^{(4)}(t), & X^{(5)} &= (X^{(2)}(t))^2 + \exp(X^{(4)}(t)) + \epsilon^{(5)}(t), \\ X^{(6)}(t) &= (0.5 + |X^{(4)}(t)|)^2 + \epsilon^{(6)}(t), & X^{(7)}(t) &= \epsilon^{(7)}(t), \\ X^{(8)}(t) &= \cos(\pi X^{(7)}(t)) + \epsilon^{(8)}(t), & X^{(9)}(t) &= \epsilon^{(9)}(t), \\ X^{(10)}(t) &= 5(X^{(3)}(t))^3 + \epsilon^{(10)}(t). \end{aligned}$$

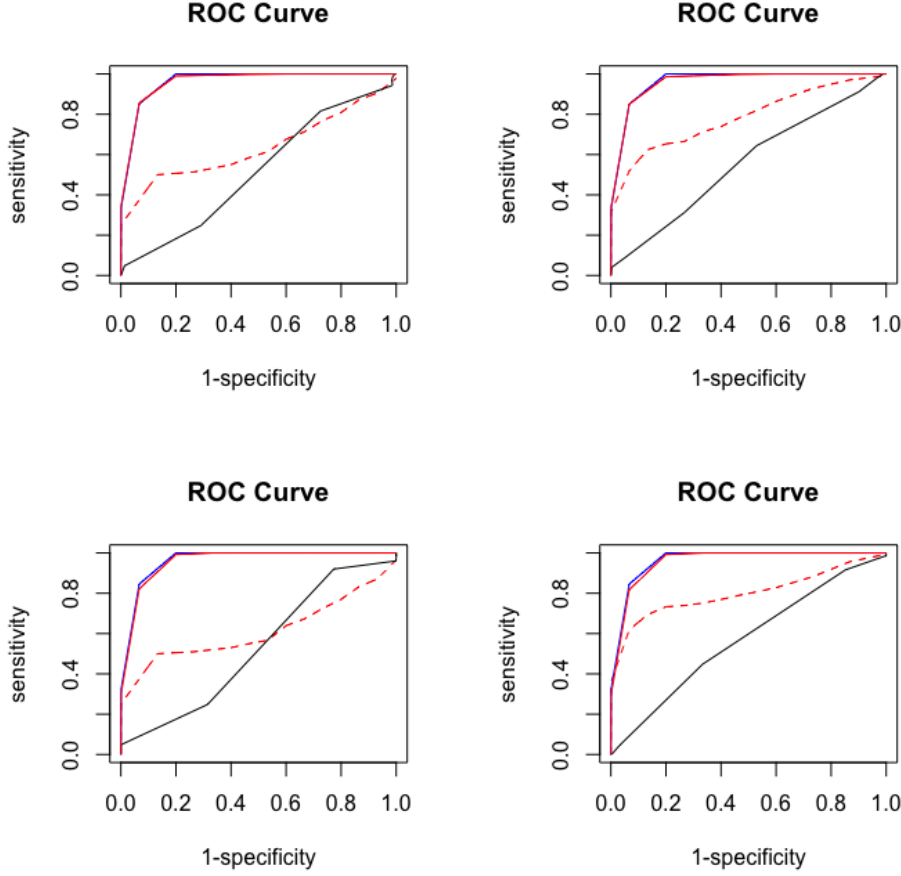


Figure 2: ROC curves for four estimators. Upper left: balanced case with $n = 100$; lower left: balanced case with $n = 200$; upper right: unbalanced case with $n = 100$; lower right: unbalanced case with $n = 200$.

where $\epsilon^{(1)}, \dots, \epsilon^{(1)}$ are independent random from which generated in the same way as in Model I. Here the edge set is $E = \{(1, 3), (3, 10), (2, 5), (2, 4), (4, 5), (4, 6), (7, 8)\}$. The ROC curves and AUC values are shown in Figure 3 and Table 2. As we observe, f-SGM performs the best. Again, the performance of f-SGM and FAPO are quite similar, and they are significantly better than the other two methods.

Time	n	n-SGM	FAPO	f-SGM	FGGM
Balanced	100	0.61(0.03)	0.94(0.02)	0.96(0.02)	0.42(0.02)
	200	0.62(0.04)	0.94(0.02)	0.96(0.02)	0.43(0.01)
Unbalanced	100	0.76(0.04)	0.94(0.02)	0.95(0.02)	0.41(0.02)
	200	0.77(0.05)	0.94(0.02)	0.95(0.02)	0.44(0.02)

Table 2: AUC results for model II.

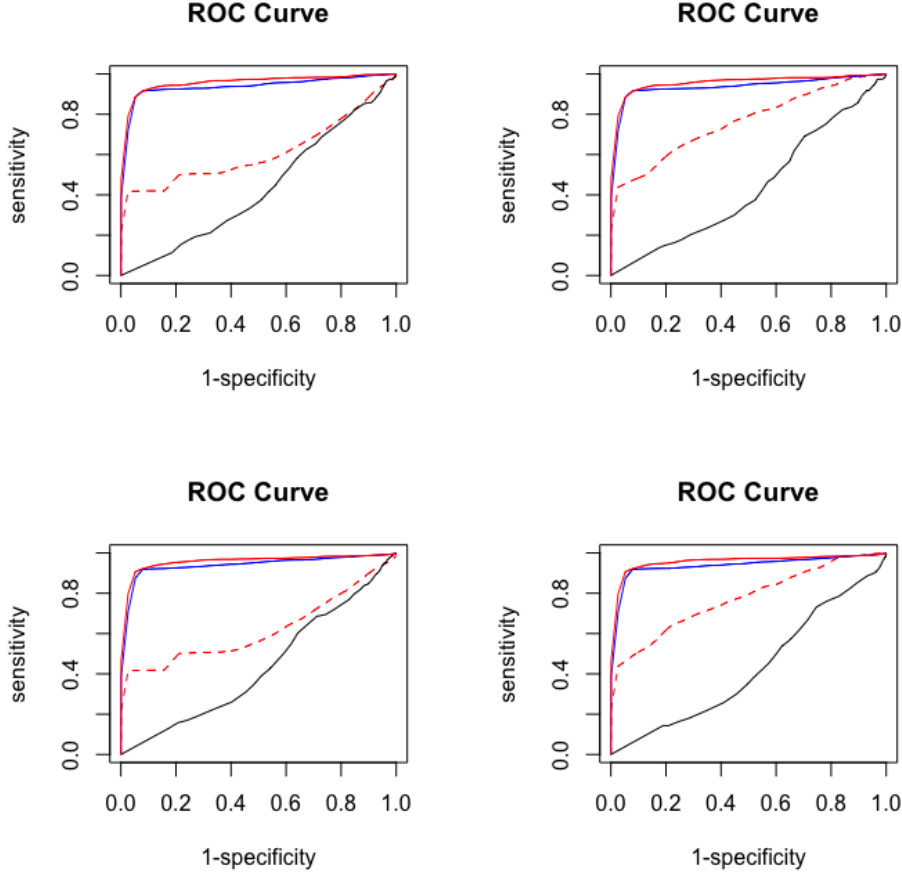


Figure 3: ROC curves for four estimators. Upper left: balanced case with $n = 100$; lower left: balanced case with $n = 200$; upper right: unbalanced case with $n = 100$; lower right: unbalanced case with $n = 200$.

6.2 Nonlinear models with heteroscedasticity

Model III. Consider the nonlinear model with heteroscedasticity:

$$\begin{aligned} X^{(1)}(t) &= \epsilon^{(1)}(t), & X^{(2)}(t) &= \epsilon^{(2)}(t), & X^{(3)}(t) &= \sin(\pi X^{(1)}(t))\epsilon^{(3)}(t), \\ X^{(4)}(t) &= (1 + 0.5|X^{(2)}(t)|)^3\epsilon^{(4)}(t), & X^{(5)}(t) &= 3(X^{(2)}(t))^2\epsilon^{(5)}(t), \end{aligned}$$

where $\epsilon^{(1)}, \dots, \epsilon^{(5)}$ are generated in the same way as the previous model. In this model the random functions depend on each other through the conditional variance rather than the conditional mean, as in the previous two models. One of the main advantages of f-SGM is that it can capture the dependence beyond the conditional mean. The FAPO, due to its additive nature, is less effective under such circumstances. The true edge set of model III is $E = \{(1, 3), (2, 4), (2, 5)\}$. Figure 4 and Table 3 show the ROC curves and AUC values. In this case, f-SGM significantly outperform all other methods.

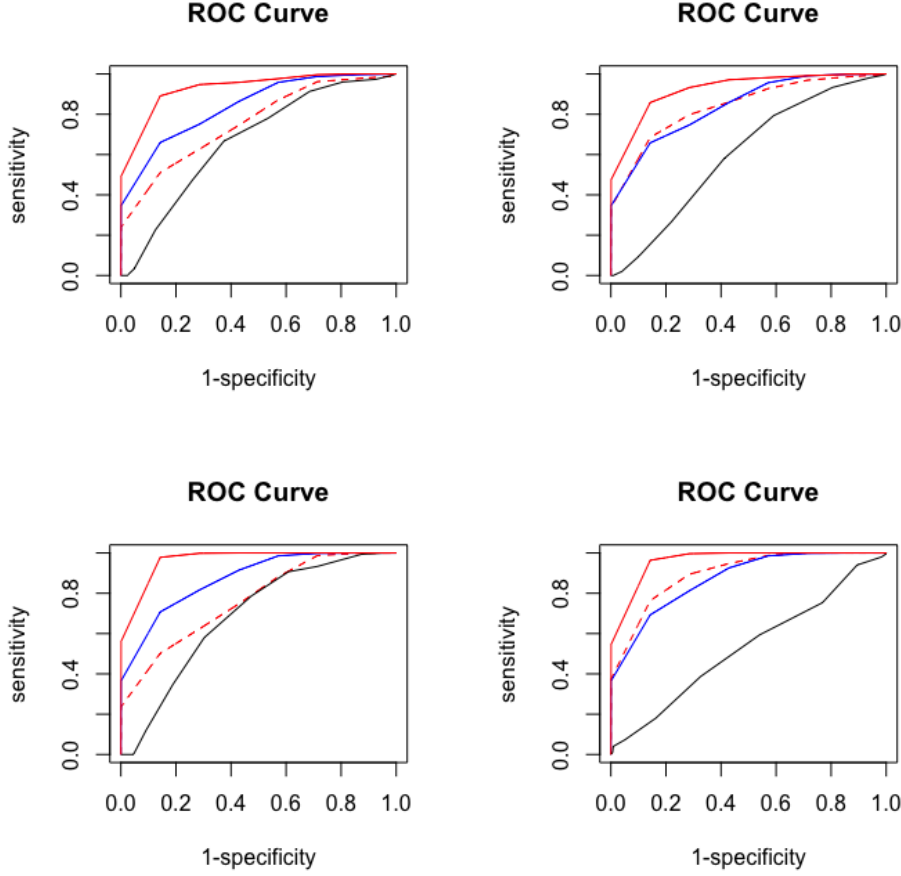


Figure 4: ROC curves for four estimators. Upper left: balanced case with $n = 100$; lower left: balanced case with $n = 200$; upper right: unbalanced case with $n = 100$; lower right: unbalanced case with $n = 200$.

Time	n	n-SGM	FAPO	f-SGM	FGGM
Balanced	100	0.77(0.08)	0.86(0.03)	0.95(0.05)	0.68(0.13)
	200	0.78(0.07)	0.89(0.03)	0.99(0.01)	0.69(0.10)
Unbalanced	100	0.86(0.09)	0.86(0.04)	0.94(0.04)	0.61(0.14)
	200	0.92(0.03)	0.89(0.03)	0.98(0.01)	0.54(0.14)

Table 3: AUC results for model III.

6.3 Gaussian model

We next compare f-SGM, FAPO, FGGM, and n-SGM under the Gaussian assumption to see how much information we lose as compared with the parametric model under the Gaussian assumption. This model is taken from Qiao et al. (2019), Li and Solea (2018).

Model IV. We generate $X^{(i)}(t), i = 1, \dots, 5$ from the following model:

$$X^{(i)}(t) = \sum_{k=1}^s \xi_{ik} u_{ik}(t), \quad i = 1, \dots, p, \quad s = 5.$$

where $\{u_{ik}(t), k = 1, 2, 3, 4, 5\}$ are from the first five functions in the Fourier basis

$$1, \quad \sqrt{2} \sin(2\pi t), \quad \sqrt{2} \cos(2\pi t), \quad \sqrt{2} \sin(4\pi t), \quad \sqrt{2} \cos(4\pi t),$$

and $\xi = (\xi_{11}, \dots, \xi_{15}, \dots, \xi_{p1}, \dots, \xi_{p5})^\top$ is multivariate Gaussian with mean 0 and block precision matrix $\Theta = \mathbb{R}^{5p \times 5p}$

$$\Theta_{ij} = \begin{cases} I_5 & \text{if } i = j, \\ 0.5I_5 & \text{if } |i - j| = 1, \\ 0.3I_5 & \text{if } |i - j| = 2, \\ 0 & \text{otherwise.} \end{cases}$$

As we can see from Figure 5 and Table 4, FGGM performs better than the three nonparametric methods, as expected. However, f-SGM shows a clear advantage compared to FAPO, which means f-SGM loses less information than FAPO in the Gaussian model.

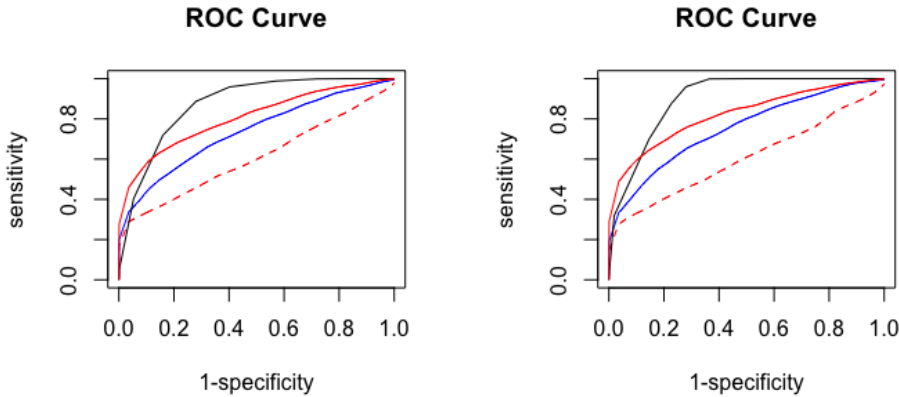


Figure 5: ROC curves for model IV. Left: $n = 100$; right: $n = 200$.

n	n-SGM	FAPO	f-SGM	FGGM
100	0.61 (0.07)	0.74 (0.07)	0.80 (0.04)	0.87 (0.03)
200	0.61 (0.07)	0.75 (0.05)	0.82 (0.04)	0.90 (0.02)

Table 4: AUC results for model IV.

6.4 Increased dimensions and sample sizes

We next repeat the comparisons for Models I, III, and IV by increasing the sample size ($n = 100, 200, 300$), and dimension ($p = 20, 30, 40$). We omit Model II as it is similar to

Model I. We increase p by adding new nodes and edges to Model I, III, and IV as described below. For Model I with $p = 20$, we add the nodes $11, \dots, 20$ and the following edges

$$\text{Model I}' : X^{(13)}(t) = (0.5 + |X^{(17)}(t)|)^3 + \epsilon^{(13)}(t), \quad X^{(16)}(t) = \exp(X^{(19)}(t)) + \epsilon^{(16)}(t), \\ X^{(18)}(t) = \sin(\pi X^{(12)}(t)) + \epsilon^{(18)}(t).$$

For $p = 30$, we further add the nodes $21, \dots, 30$ and the edges

$$\text{Model I}'' : X^{(21)}(t) = (X^{(26)}(t))^2 + \epsilon^{(21)}(t), \quad X^{(24)}(t) = \cos(\pi X^{(23)}(t)) + \epsilon^{(24)}(t), \\ X^{(27)}(t) = (0.5 + |X^{(22)}(t)|)^2 + \epsilon^{(27)}(t), \quad X^{(29)}(t) = \exp(X^{(23)}(t)) + \epsilon^{(29)}(t).$$

For $p = 40$, we further add the nodes $31, \dots, 40$ and the edges

$$\text{Model I}''' : X^{(35)}(t) = (X^{(31)}(t))^2 + \epsilon^{(35)}(t), \quad X^{(38)}(t) = \cos(\pi X^{(37)}(t)) + \epsilon^{(38)}(t).$$

For Model III with $p = 20$, we add nodes $11, \dots, 20$ and the following edges

$$\text{Model III}' : X^{(10)}(t) = \exp(|X^{(7)}(t)|)\epsilon^{(10)}(t), \quad X^{(14)}(t) = (0.3 + |X^{(9)}(t)|)^2\epsilon^{(14)}(t), \\ X^{(15)}(t) = (0.5 + |X^{(8)}(t)|)^2\epsilon^{(15)}(t), \quad X^{(18)}(t) = 3(X^{(11)}(t))^3\epsilon^{(18)}(t).$$

For $p = 30$, we further add nodes $21, \dots, 30$ and the edges

$$\text{Model III}'' : X^{(20)}(t) = \exp(|X^{(24)}(t)|)\epsilon^{(20)}(t), \quad X^{(22)}(t) = (0.5 + |X^{(19)}(t)|)^2\epsilon^{(22)}(t), \\ X^{(26)}(t) = 3(X^{(29)}(t))^3\epsilon^{(26)}(t), \quad X^{(27)}(t) = \cos(\pi X^{(22)}(t))\epsilon^{(26)}(t).$$

For $p = 40$ we further add nodes $31, \dots, 40$ and the edges

$$\text{Model III}''' : X^{(32)}(t) = 3(X^{(38)}(t))^2\epsilon^{(32)}(t), \quad X^{(39)}(t) = (1 + |X^{(35)}(t)|)^2\epsilon^{(39)}(t).$$

For the Gaussian model (Model IV) with $p = 20, 30, 40$ we simply increase the dimension of the block precision matrix. We label these as IV', IV'', IV''. Table 5 shows the AUC values of the estimates for these models for the balanced cases. We see that superiority of f-SGM holds up very well against the increased in the network size.

Model	p	n	n-SGM	FAPO	f-SGM	FGGM
I'	20	100	0.82 (0.03)	0.96 (0.01)	0.98 (0.01)	0.74 (0.08)
		200	0.81 (0.03)	0.98 (0.01)	0.99 (0.01)	0.75 (0.09)
		300	0.79 (0.03)	0.98 (0.00)	0.99 (0.00)	0.76 (0.08)
I''	30	100	0.81 (0.03)	0.95 (0.00)	0.98 (0.01)	0.73 (0.07)
		200	0.80 (0.03)	0.97 (0.00)	0.99 (0.00)	0.73 (0.06)
		300	0.80 (0.03)	0.98 (0.00)	0.99 (0.00)	0.71 (0.07)
I'''	40	100	0.81 (0.02)	0.95 (0.00)	0.98 (0.00)	0.72 (0.06)
		200	0.80 (0.02)	0.97 (0.00)	0.99 (0.00)	0.73 (0.06)
		300	0.80 (0.01)	0.98 (0.00)	0.99 (0.00)	0.73 (0.06)
III'	20	100	0.84 (0.04)	0.94 (0.01)	0.97 (0.01)	0.73 (0.07)
		200	0.87 (0.04)	0.95 (0.00)	0.99 (0.00)	0.72 (0.08)
		300	0.87 (0.03)	0.96 (0.01)	0.99 (0.00)	0.73 (0.07)
III''	30	100	0.83 (0.02)	0.94 (0.00)	0.97 (0.00)	0.73 (0.05)
		200	0.83 (0.02)	0.95 (0.01)	0.98 (0.00)	0.75 (0.05)
		300	0.84 (0.01)	0.96 (0.01)	0.99 (0.00)	0.75 (0.05)
III'''	40	100	0.85 (0.01)	0.95 (0.01)	0.97 (0.00)	0.71 (0.06)
		200	0.85 (0.02)	0.96 (0.01)	0.99 (0.00)	0.76 (0.05)
		300	0.85 (0.01)	0.97 (0.00)	0.99 (0.00)	0.75 (0.05)
IV'	20	100	0.61 (0.02)	0.73 (0.04)	0.79 (0.03)	0.92 (0.01)
		200	0.60 (0.03)	0.74 (0.03)	0.82 (0.02)	0.95 (0.01)
		300	0.61 (0.03)	0.75 (0.03)	0.85 (0.02)	0.95 (0.01)
IV''	30	100	0.60 (0.02)	0.69 (0.03)	0.77 (0.02)	0.94 (0.01)
		200	0.60 (0.02)	0.74 (0.02)	0.81 (0.02)	0.97 (0.00)
		300	0.75 (0.03)	0.74 (0.02)	0.85 (0.02)	0.97 (0.01)
IV'''	40	100	0.60 (0.02)	0.69 (0.03)	0.76 (0.02)	0.95 (0.01)
		200	0.60 (0.02)	0.74 (0.02)	0.81 (0.02)	0.97 (0.01)
		300	0.60 (0.02)	0.74 (0.02)	0.83 (0.01)	0.98 (0.00)

Table 5: AUC results for extended models

7 Application

7.1 f-MRI dataset

We now apply our method to an f-MRI human brain imaging dataset in the ADHD consortium (Milham et al., 2012), which is released by Neuro Bureau, a neuroscience collaborative that supports open neuroscience research. The version we used is preprocessed by the Athena pipeline. This dataset is available at

https://www.nitrc.org/ftrs/?group_id=383.

The dataset consists of observations from 171 children, which are divided into an ADHD group of 73 children and a control group of 98 children. A brain is divided into 116 regions of interest using the anatomical labelling atlas developed by Craddock et al. (2012). For each child and each brain region, the f-MRI data are observed at 172 equally spaced time

points. The f-MRI data values are extracted by averaging over all voxels within each region at each time point. Our goal of the analysis is to find the difference in the brain network structure between children with and without having ADHD. We applied f-SGM, FAPO, FGGM, and n-SGM to this dataset.

Due to the high computational cost of FGGM for high dimensional networks, we use a thresholding version of FGGM which is described in Li and Solea (2018). First, we calculate a precision matrix based on the functional principal component. Then we determine the connectivity by thresholding the operator norm of (i, j) th block of the precision matrix. We choose the threshold so that 7% of the pairs of vertices are edges. In particular, the selected threshold is 0.03 for both ADHD and control groups. For the f-SGM and FAPO methods we use the Brownian motion covariance kernel for the first-level spaces and the Gaussian radial basis kernel for the second-level spaces. For the tuning parameters we use the methods that have been discussed in Section 5.7. We also use the Gaussian radial basis kernel for the first-level spaces and cannot find any significant difference.

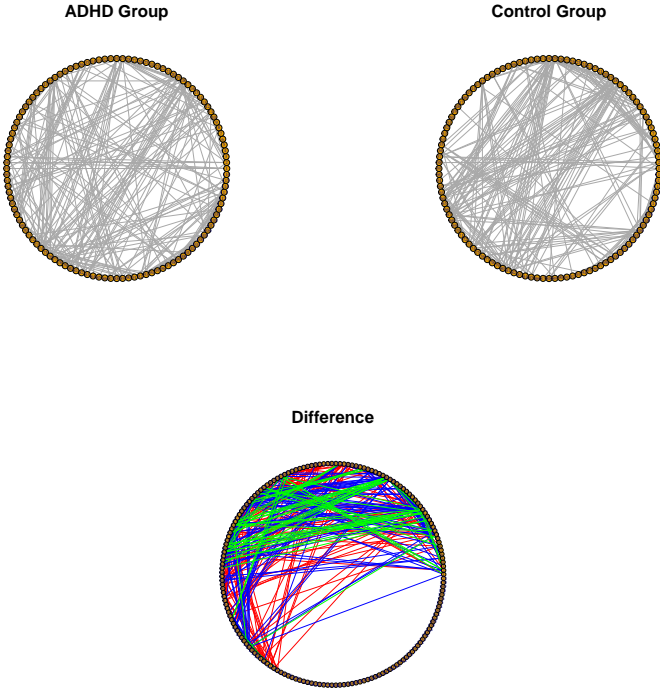


Figure 6: Brain structure between ADHD group and control group by using f-SGM

Figures 6 through 9 show the brain networks for combinations of

$$\{\text{f-SGM, FAPO, FGGM, n-SGM}\} \times \{\text{ADHD group, control group}\}.$$

For the third plot of each of Figures 6 through and 9, the red lines indicate the edges in the ADHD group but not in the control group, blue lines indicate the edges in the control group

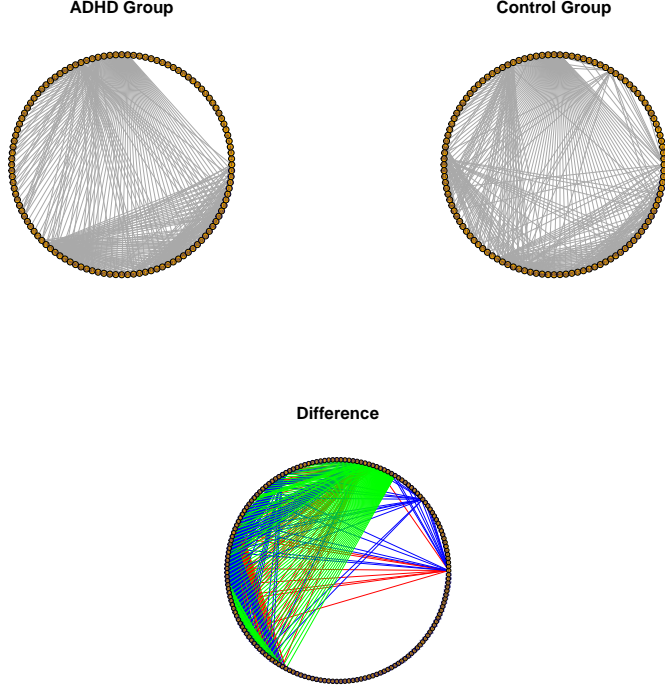


Figure 7: Brain structure between ADHD group and control group by using n-SGM

but not in the ADHD group, and green line means the common edges. We can observe a difference between the brain network structure between the ADHD group and the control group. As we can see, the f-SGM method shows the clear difference in the brain structure between ADHD and non-ADHD children.

8 Discussion

This paper incorporates the recently developed techniques of nonlinear SDR for functional data to construct a flexible nonparametric estimator of the functional graphical model. Our method does not rely on any distribution assumption and, as our simulation experiments indicate, effectively avoids the curse of dimensionality that often hampers a fully nonparametric method.

The current method is an extension of the sufficient graphical model of Li and Kim (2024) from the multivariate setting to the multivariate functional setting, which is increasingly common in modern applications, particularly in brain neurological research. The novelty in this extension lies in the use of the first-level Hilbert spaces that accommodates functional data, and the hybrid conjoined conditional covariance operator, by which we determine absence of edge. In the sufficient graphical model of Li and Kim (2024), the statistical dependence captured through the RKHS defined on the random variables in the vertices;

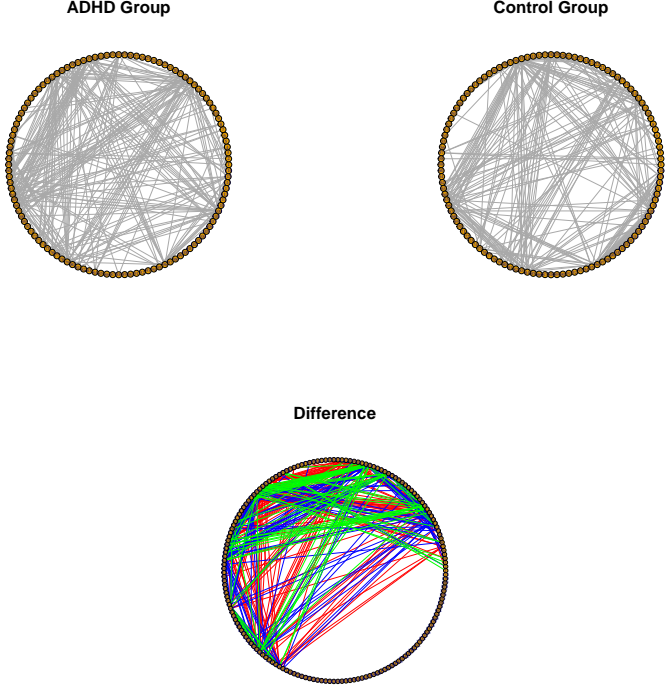


Figure 8: Brain structure between ADHD group and control group by using FAPO

whereas for the current f-SGM the statistical dependence is captured by the RKHS defined on the first-level functional spaces in which the observations on the vertices reside. The RKHS is supported on the first-level Hilbert spaces with its kernel constructed from the inner products of the first-level spaces; nonlinear SDR is then performed on the RKHS (the second-level Hilbert space). After extracting the sufficient predictors U^{ij} using f-GSIR, which is a Euclidean vector, the hybrid CCCO is then introduced to determine conditional independence. This hybrid operator involves two Hilbertian random functions and a Euclidean random vector. In comparison, the CCCO used in the sufficient graphical model of Li and Kim (2024) involves to real-valued random variables and a random vector. The implementing algorithms of Li and Kim (2024) also need to be modified to adapt to these novel structures.

The algorithms of the f-SGM are reasonably easy to implement. Essentially, we use the function GSIR as a module, and apply it repeatedly to each distinct pair vertices, which each repetition involving an eigendecomposition of an n by n matrix. The algorithms are easily parallelized for larger networks, as the computation the f-GSIR predictors and the subsequent hybrid CCCO for different pairs of vertices are independent of each other and can be distributed among a large number of different computing units. Thus, it is feasible for computing relatively large networks.

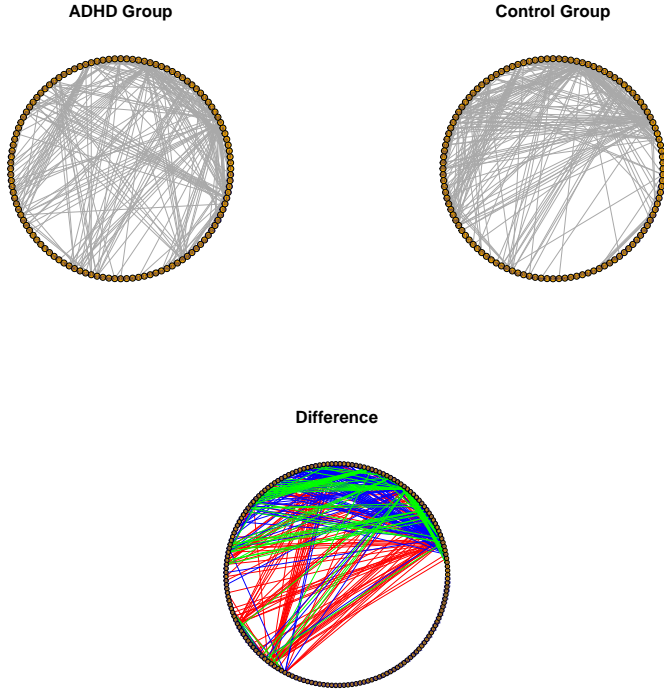


Figure 9: Brain structure between ADHD group and control group by using FGGM

While the current paper focuses on developing the methodology as well as the theoretical structure at the population level, we haven't touched on the asymptotic developments, such as estimation consistency, convergence rates, optimal tuning, order determination, and statistical inference. We leave these to future research.

References

R Bellman. Curse of dimensionality. *Adaptive control processes: a guided tour*. Princeton, NJ, 1961.

Patrick Billingsley. *Probability and measure*. John Wiley & Sons, 2008.

R Cameron Craddock, G Andrew James, Paul E Holtzheimer III, Xiaoping P Hu, and Helen S Mayberg. A whole brain fmri atlas generated via spatially constrained spectral clustering. *Human brain mapping*, 33(8):1914–1928, 2012.

Bernd Fellinghauer, Peter Bühlmann, Martin Ryffel, Michael Von Rhein, and Jan D Reinhardt. Stable graphical model estimation with random forests for discrete, continuous, and mixed variables. *Computational Statistics & Data Analysis*, 64:132–152, 2013.

Frédéric Ferraty and Philippe Vieu. *Nonparametric functional data analysis: theory and practice*. Springer Science & Business Media, 2006.

Kenji Fukumizu, Arthur Gretton, Xiaohai Sun, and Bernhard Schölkopf. Kernel measures of conditional dependence. In *Advances in neural information processing systems*, pages 489–496, 2008.

Roger A Horn and Charles R Johnson. *Matrix analysis*. Cambridge university press, 2012.

Lajos Horváth and Piotr Kokoszka. *Inference for functional data with applications*, volume 200. Springer Science & Business Media, 2012.

Tailen Hsing and Randall Eubank. *Theoretical foundations of functional data analysis, with an introduction to linear operators*. John Wiley & Sons, 2015.

Kuang-Yao Lee and Lexin Li. Functional structural equation model. *Journal of the Royal Statistical Society Series B: Statistical Methodology*, 84:600—629, 2022.

Kuang-Yao Lee, Bing Li, and Francesca Chiaromonte. A general theory for nonlinear sufficient dimension reduction: Formulation and estimation. *The Annals of Statistics*, 41(1):221–249, 2013.

Kuang-Yao Lee, Bing Li, and Hongyu Zhao. On an additive partial correlation operator and nonparametric estimation of graphical models. *Biometrika*, 103(3):513–530, 2016a.

Kuang-Yao Lee, Bing Li, and Hongyu Zhao. Variable selection via additive conditional independence. *Journal of the Royal Statistical Society. Series B (Statistical Methodology)*, pages 1037–1055, 2016b.

Kuang-Yao Lee, Dingjue Ji, Lexin Li, Todd Constable, and Hongyu Zhao. Conditional functional graphical models. *Journal of the American Statistical Association*, 118:257–271, 2023a.

Kuang-Yao Lee, Lexin Li, Bing Li, and Hongyu Zhao. Nonparametric functional graphical modeling through functional additive regression operator. *Journal of the American Statistical Association*, 118:1718–1732, 2023b.

Bing Li. *Sufficient dimension reduction: Methods and applications with R*. CRC Press, 2018.

Bing Li and Kyongwon Kim. Sufficient graphical models. *Journal of Machine Learning Research*, 25:1–64, 2024.

Bing Li and Eftychia Solea. A nonparametric graphical model for functional data with application to brain networks based on fmri. *Journal of the American Statistical Association*, pages 1–19, 2018.

Bing Li and Jun Song. Nonlinear sufficient dimension reduction for functional data. *The Annals of Statistics*, 45(3):1059–1095, 2017.

Bing Li, Hyonho Chun, and Hongyu Zhao. On an additive semigraphoid model for statistical networks with application to pathway analysis. *Journal of the American Statistical Association*, 109(507):1188–1204, 2014.

Kuang-Yao Li, Lexin Li, and B. Li. Functional directed acyclic graphs. *Journal of Machine Learning Research*, 25:1–48, 2024.

Han Liu, John Lafferty, and Larry Wasserman. The nonparanormal: Semiparametric estimation of high dimensional undirected graphs. *Journal of Machine Learning Research*, 10(Oct):2295–2328, 2009.

Han Liu, Fang Han, Ming Yuan, John Lafferty, and Larry Wasserman. The nonparanormal skeptic. *arXiv preprint arXiv:1206.6488*, 2012.

Nicolai Meinshausen, Peter Bühlmann, et al. High-dimensional graphs and variable selection with the lasso. *Annals of statistics*, 34(3):1436–1462, 2006.

Michael P Milham, Damien Fair, Maarten Mennes, Stewart HMD Mostofsky, et al. The adhd-200 consortium: a model to advance the translational potential of neuroimaging in clinical neuroscience. *Frontiers in systems neuroscience*, 6:62, 2012.

Xinghao Qiao, Shaojun Guo, and Gareth M James. Functional graphical models. *Journal of the American Statistical Association*, pages 211–222, 2019.

Xinghao Qiao, Cheng Qian, Gareth M. James, and Shaojun Guo. Doubly functional graphical models in high dimensions. *Biometrika*, pages 415—431, 2020.

James O Ramsay and Bernard W Silverman. Functional data analysis. 2005.

James O Ramsay and Bernard W Silverman. *Applied functional data analysis: methods and case studies*. Springer, 2007.

Eftychia Solea and Holger Dette. Nonparametric and high-dimensional functional graphical models. *Electronic Journal of Statistics*, 16:6175–6231, 2022.

Eftychia Solea and Bing Li. Copula gaussian graphical models for functional data. *Journal of the American Statistical Association*, pages 781–793, 2022.

Arend Voorman, Ali Shojaie, and Daniela Witten. Graph estimation with joint additive models. *Biometrika*, 101(1):85–101, 2014.

Jane-Ling Wang, Jeng-Min Chiou, and Hans-Georg Müller. Functional data analysis. *Annual Review of Statistics and Its Application*, 3:257–295, 2016.

Mingrui Xia, Jinhui Wang, and Yong He. Brainnet viewer: a network visualization tool for human brain connectomics. *PloS one*, 8(7):e68910, 2013.

Lingzhou Xue and Hui Zou. Regularized rank-based estimation of high-dimensional non-paranormal graphical models. *The Annals of Statistics*, 40(5):2541–2571, 2012.

Fang Yao, Hans-Georg Müller, and Jane-Ling Wang. Functional data analysis for sparse longitudinal data. *Journal of the American Statistical Association*, 100(470):577–590, 2005.

Ming Yuan and Yi Lin. Model selection and estimation in regression with grouped variables. *Journal of the Royal Statistical Society: Series B (Statistical Methodology)*, 68(1):49–67, 2006.

Ming Yuan and Yi Lin. Model selection and estimation in the gaussian graphical model. *Biometrika*, 94(1):19–35, 2007.

Boxin Zhao, Y. Samuel Wang, and Mladen Kolar. Direct estimation of differential functional graphical models. *Proceedings of the 33rd International Conference on Neural Information Processing Systems*, 231:2575 – 2585, 2019.

Boxin Zhao, Percy S. Zhai, Y. Samuel Wang, and Mladen Kolar. High-dimensional functional graphical model structure learning via neighborhood selection approach. *Electronic Journal of Statistics*, 18:1042–1129, 2024.

Hongxiao Zhu, Nate Strawn, and David B Dunson. Bayesian graphical models for multivariate functional data. *The Journal of Machine Learning Research*, 17(1):7157–7183, 2016.